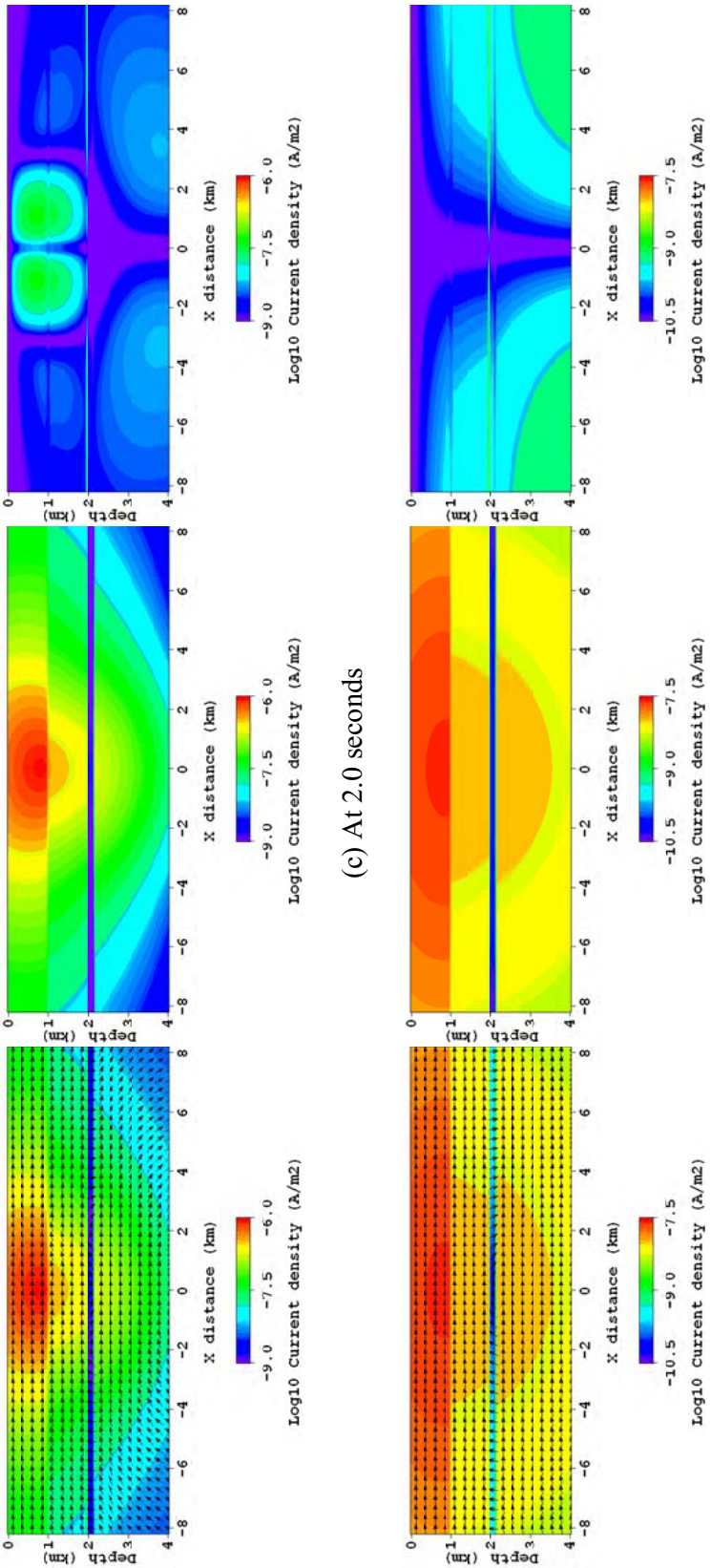

(c) At 2.0 seconds

(d) At 20 seconds

Figure 5.31 Continued.

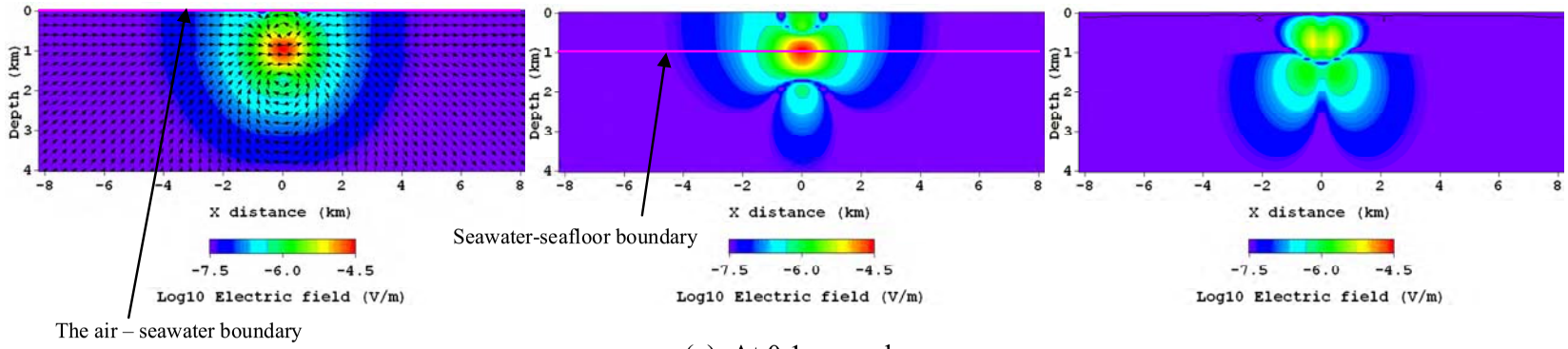

(a) At 0.1 seconds

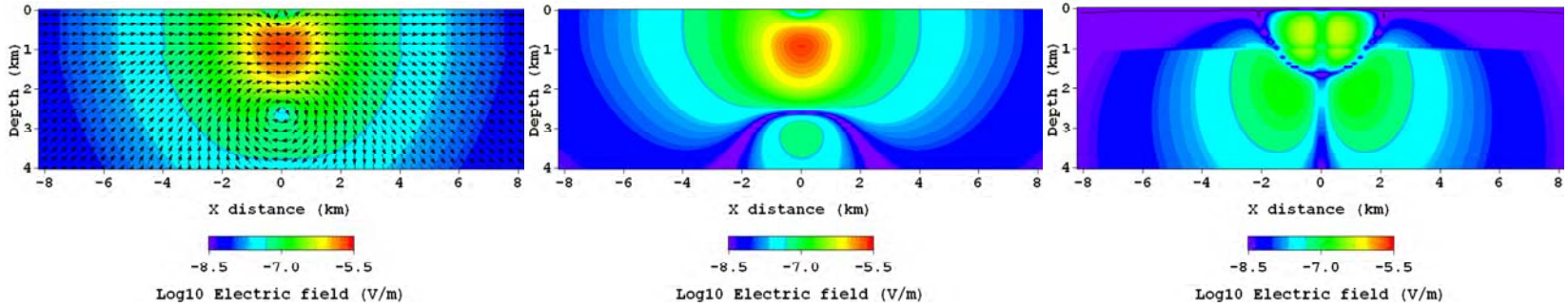

(b) At 0.5 seconds

Figure 5.32. Electric field distribution snapshots at four different measurement times on the xz cross-section for the background model with a 250m long x-oriented time-domain HED source at (0 m, 0 m, 950 m). Total electric field (left), horizontal electric field (middle) and vertical electric field (right).

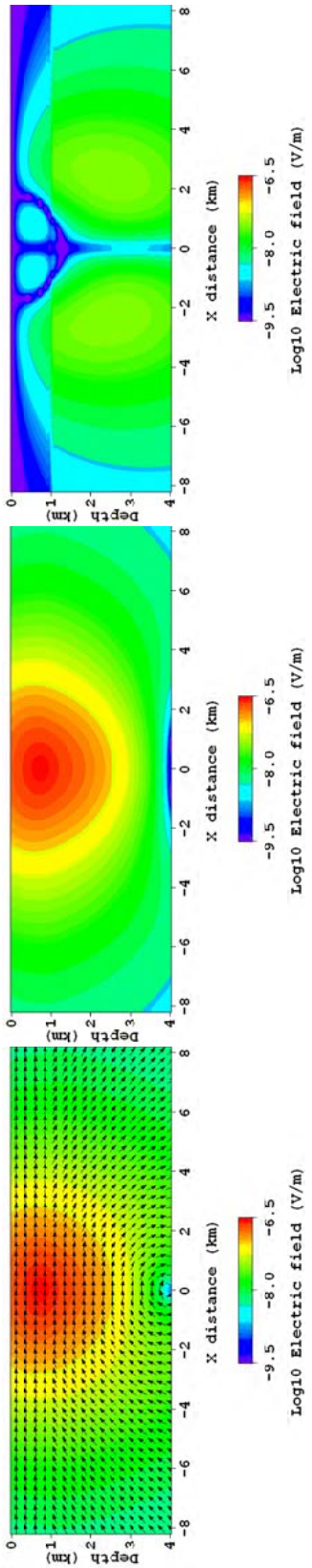

(c) At 2.0 seconds

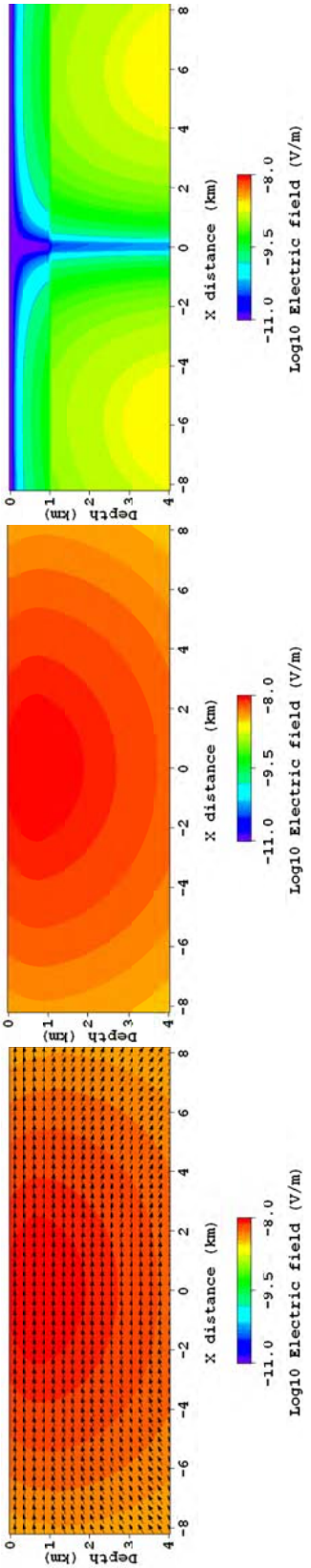

(d) At 20 seconds

Figure 5.32 Continued.

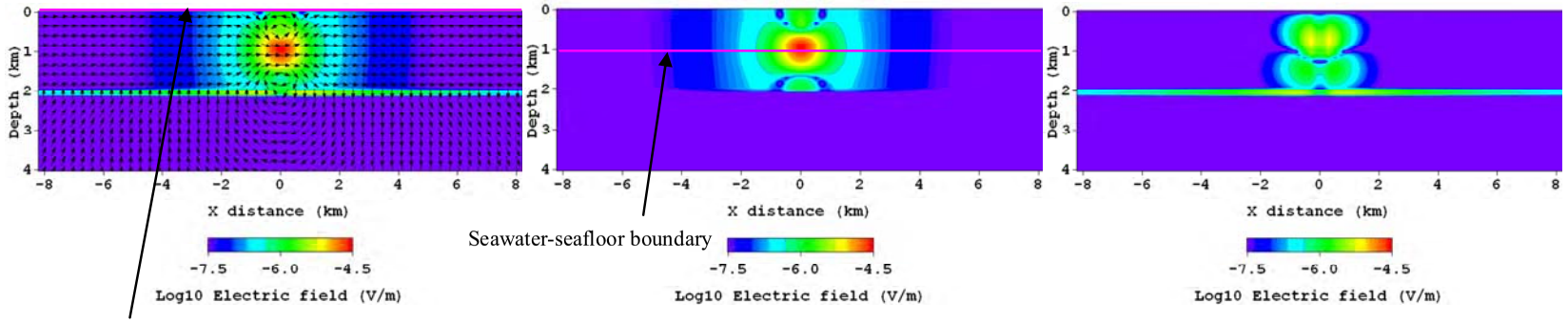

(a) At 0.1 seconds

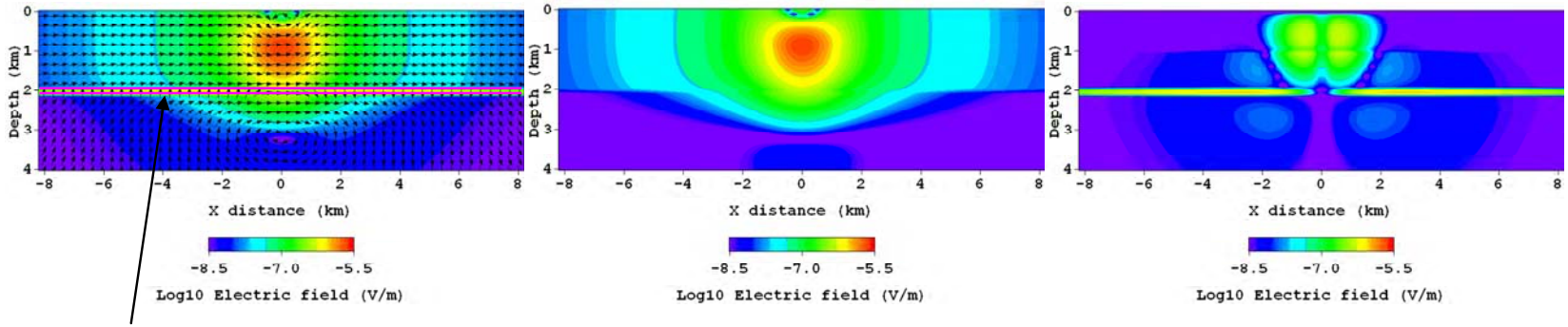

(b) At 0.5 seconds

Figure 5.33. Electric field distribution snapshots at four different measurement times on the xz cross-section for the 1-D model with a 250m long x-oriented time-domain HED source at (0 m, 0 m, 950 m). Total electric field (left), horizontal electric field (middle) and vertical electric field (right).

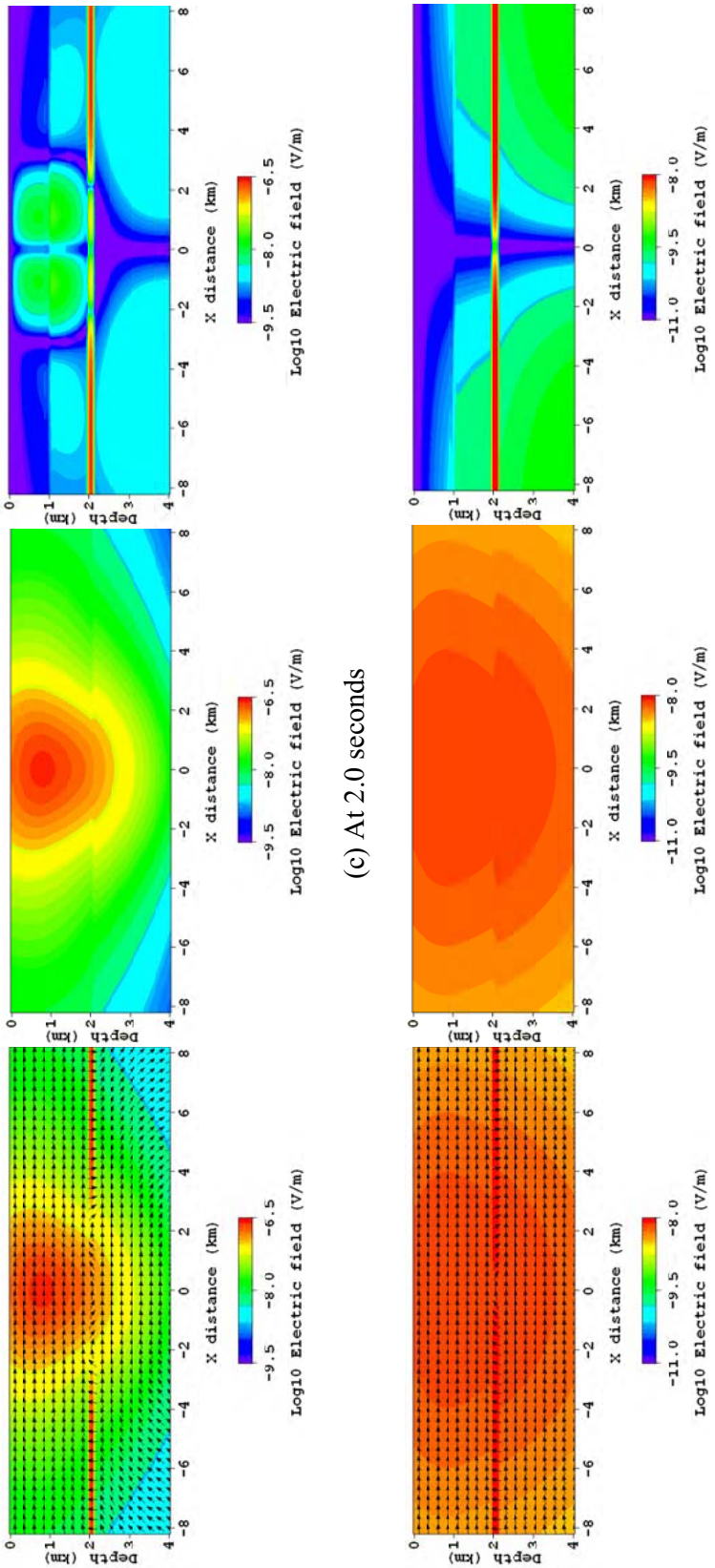

(c) At 2.0 seconds

(d) At 20 seconds

Figure 5.33 Continued.

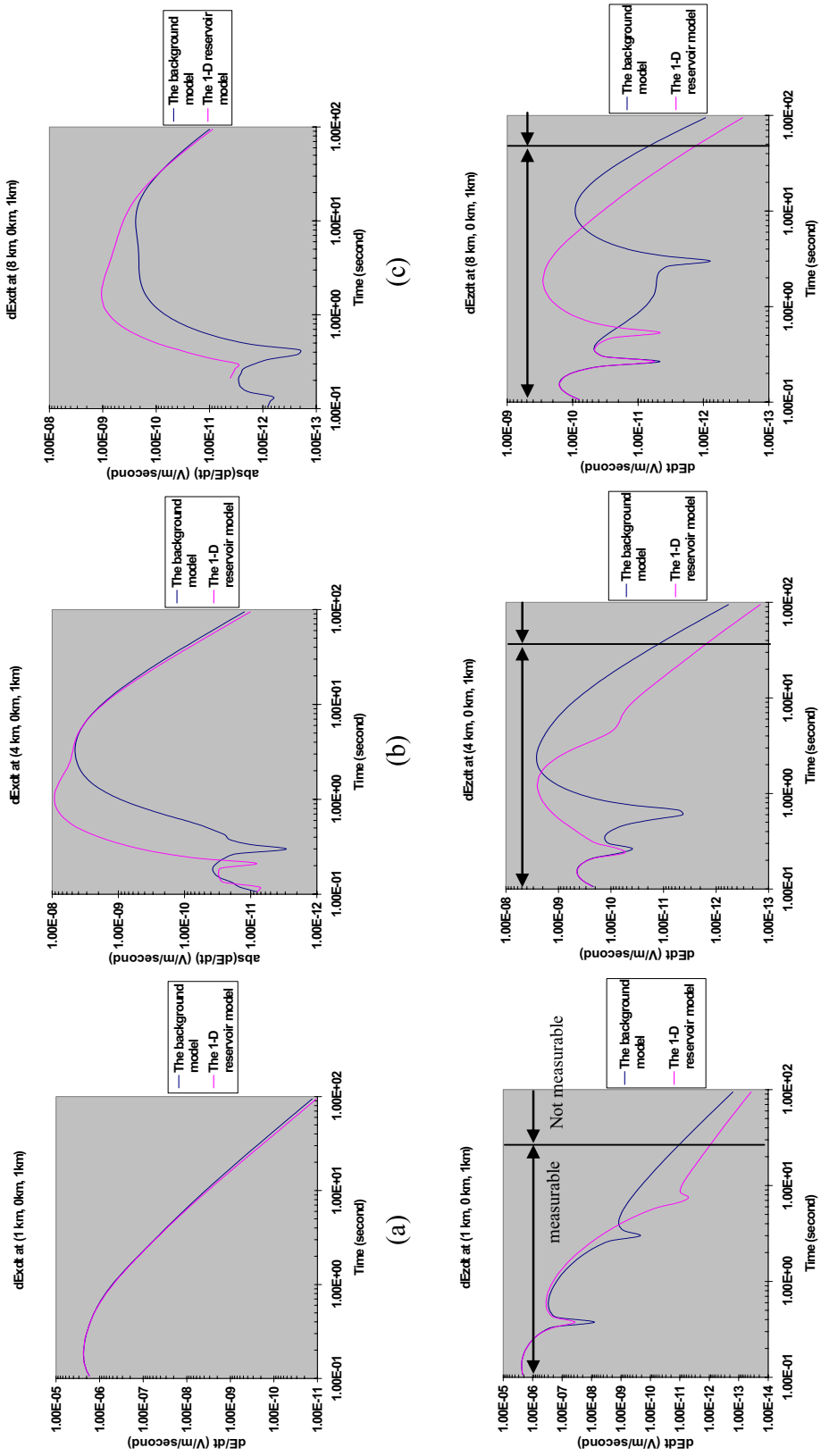

Figure 5.34. The time-derivatives of the in-line E_X and E_Z responses at different receiver locations the using the marine TDCSEM method.

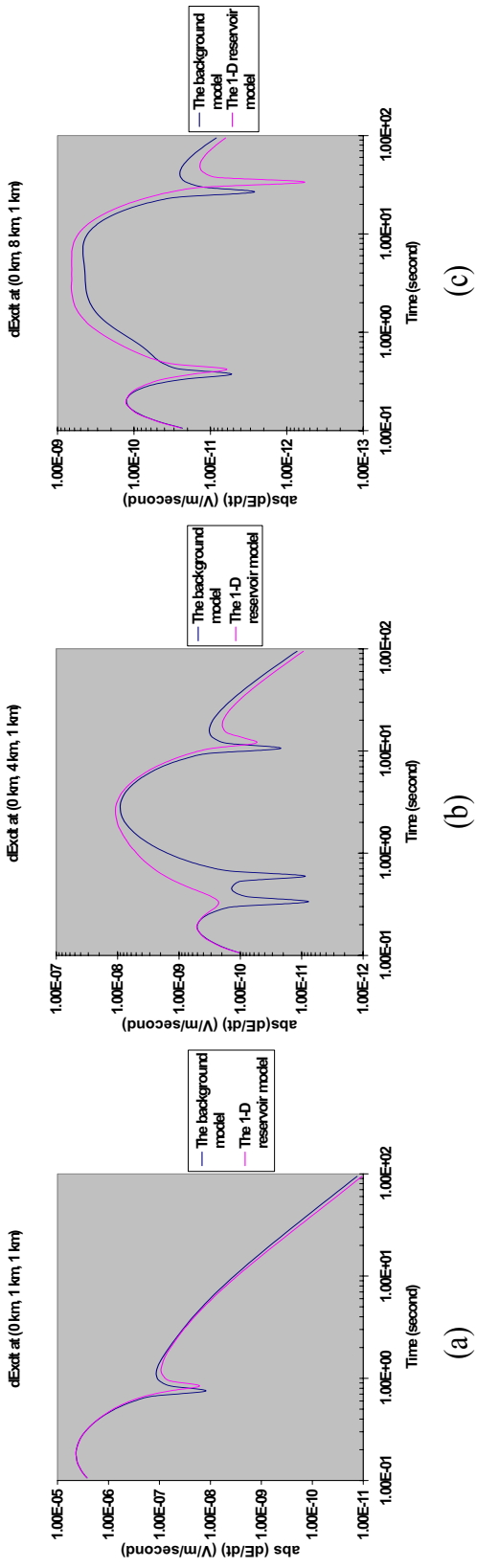

Figure 5.35. The time-derivatives of the broadside E_X responses at different receiver locations using the marine TDCSEM method.

(a) The FDCSEM method (source frequency: 0.63 Hz) (b) The TDCSEM method (source-receiver separation: 6km)

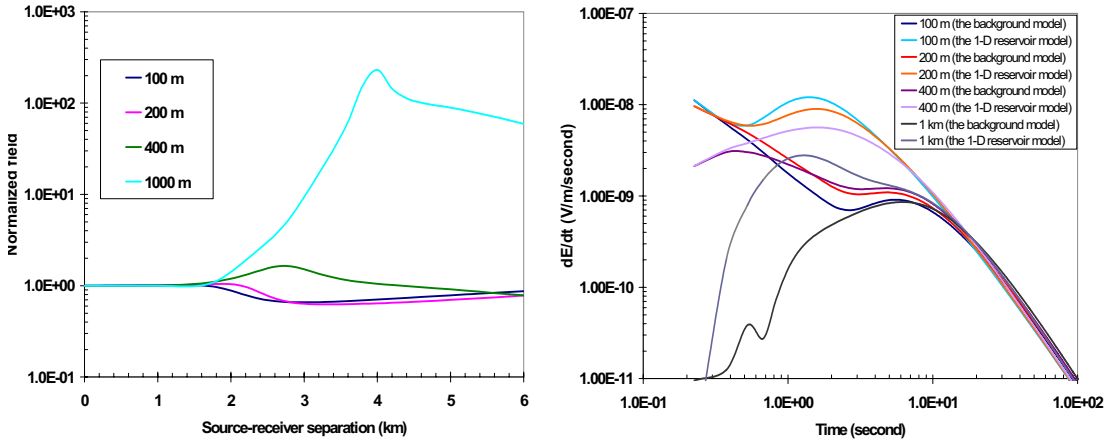

Figure 5.36. The 1-D FDCSEM and TDCSEM responses with varying depth of seawater. The four different seawater depths (100 m, 200 m, 400 m and 1000 m) are considered here. The previous 1-D hydrocarbon reservoir is embedded a depth of 1km below the seafloor.

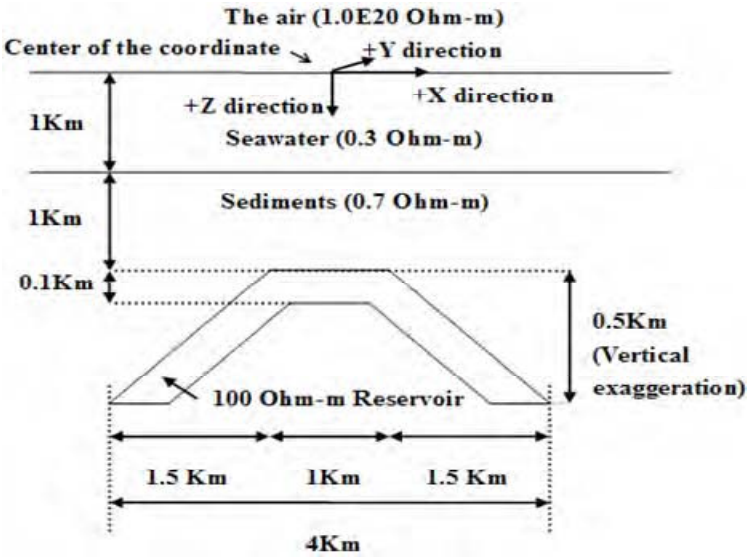

(a) Cross-sectional view

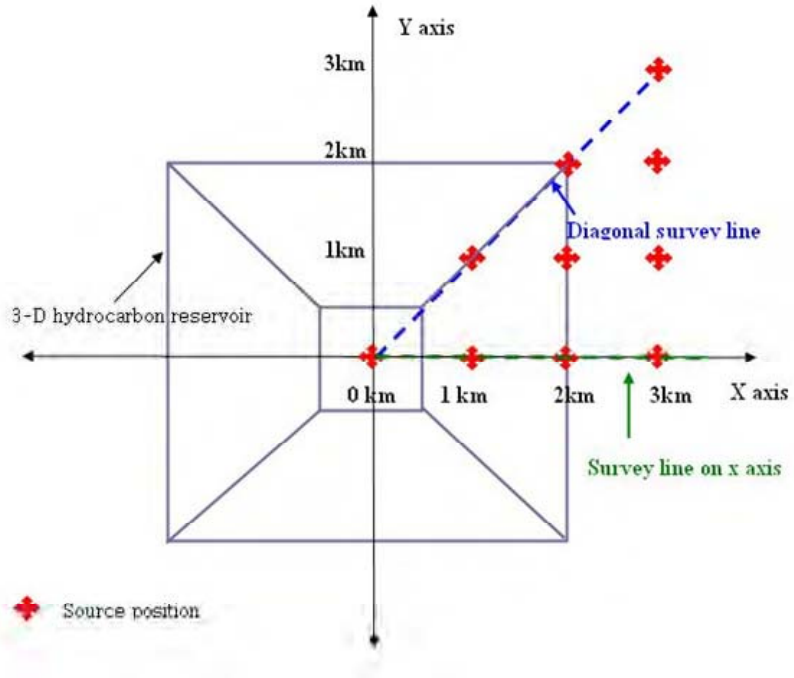

(b) Plan view

Figure 5.37. The 3-D hydrocarbon reservoir model and the survey configuration. (a) the cross-sectional view of the 3-D hydrocarbon reservoir, and (b) the plan view of the 3-D hydrocarbon reservoir.

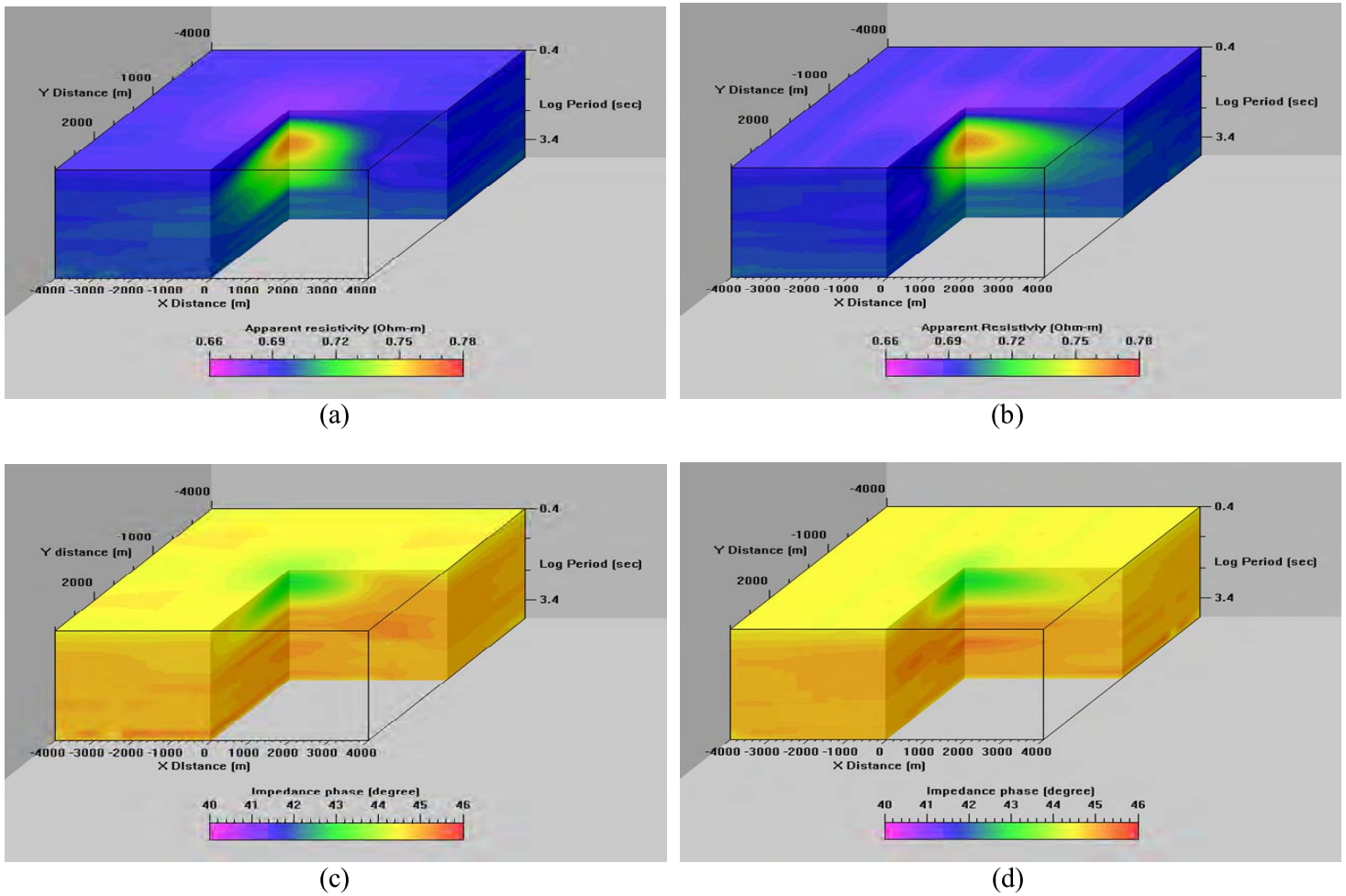

Figure 5.38. Volume representation of pseudo-sections for the MMT forward modeling of the 3-D reservoir model. (a) Z_{XY} apparent resistivity, (b) Z_{YX} apparent resistivity, (c) Z_{XY} impedance phase and (d) Z_{YX} impedance phase.

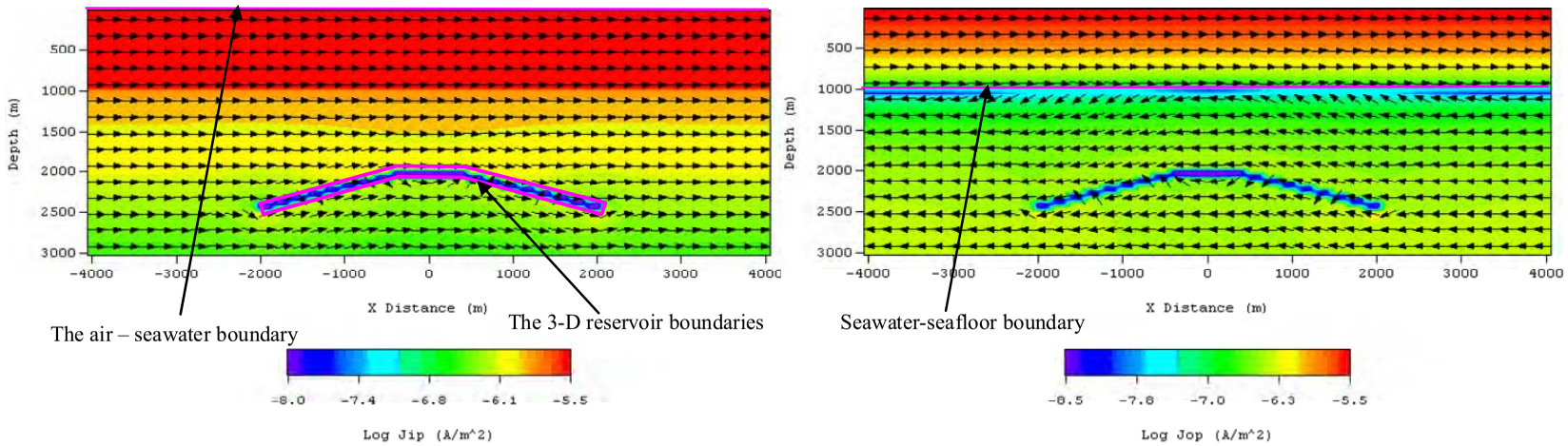

(a) In-phase (left) and out-of phase (right) current density vector field

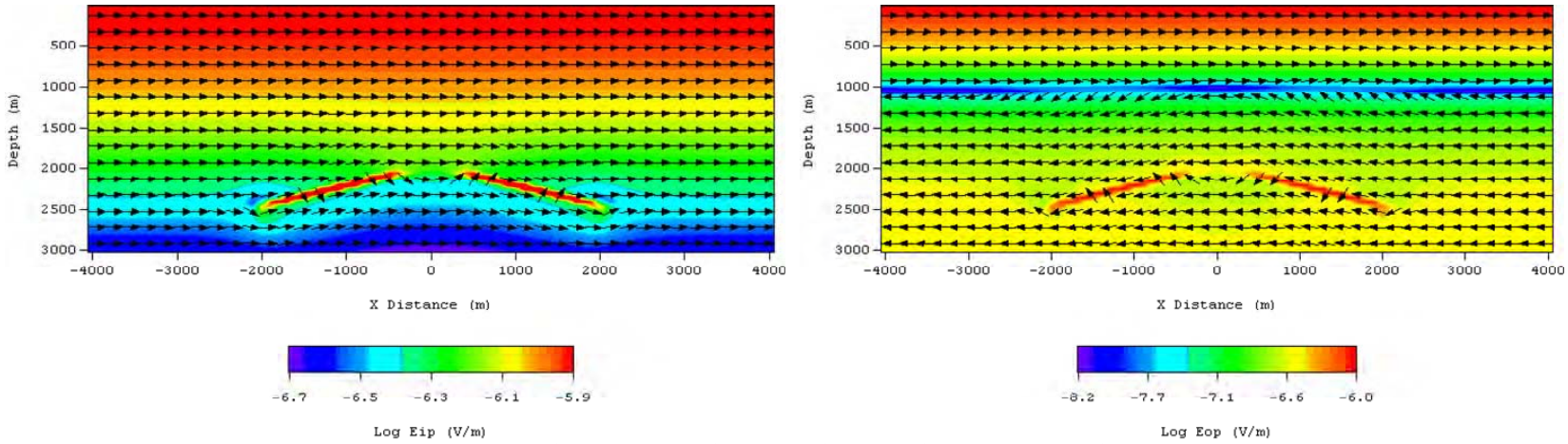

(b) in-phase (left) and out-of-phase (right) electric field

Figure 5.39. Z_{XY} electric field and current density distributions due to 0.04 Hz MMT plane wave source for the 3-D reservoir model. (a) In-phase and out-of phase current density vector field, and (b) in-phase and out-of-phase electric field.

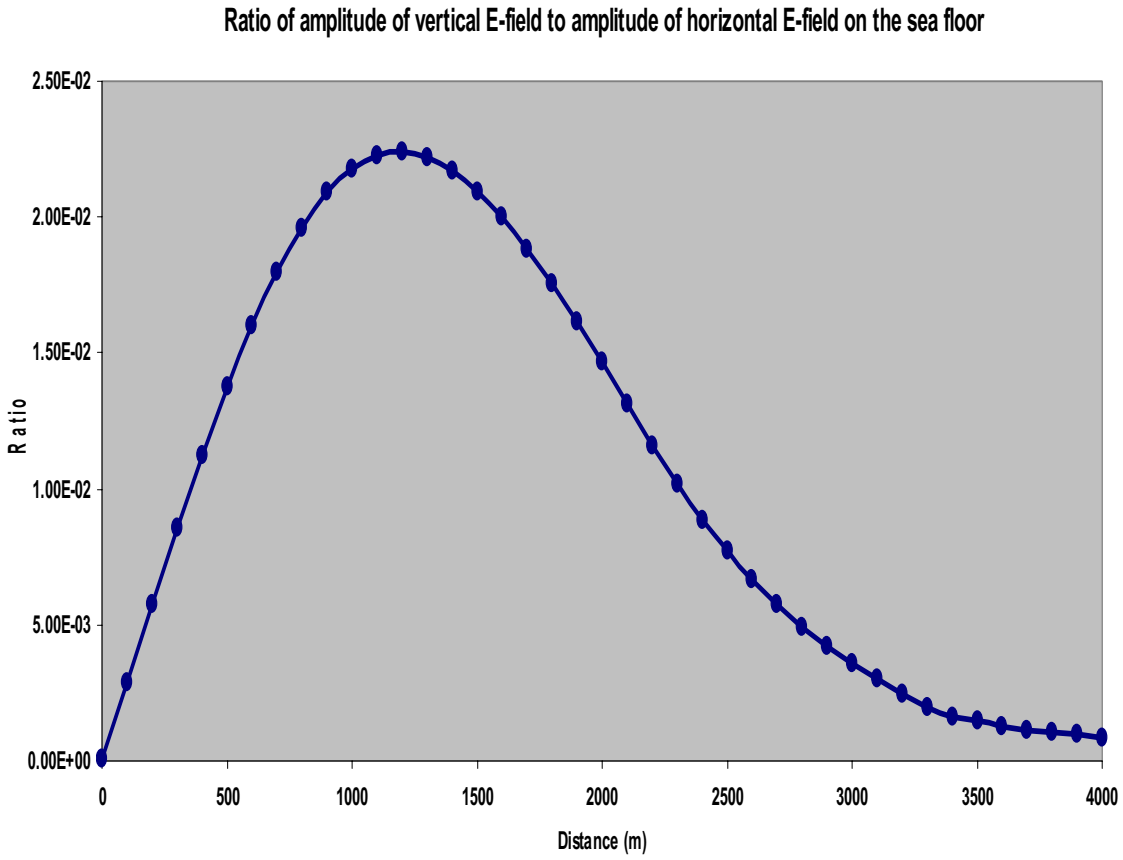

Figure 5.40. The ratio of the vertical electric field to the horizontal electric field due to 0.04 Hz MMT plane wave source on the seafloor for the 3-D reservoir model.

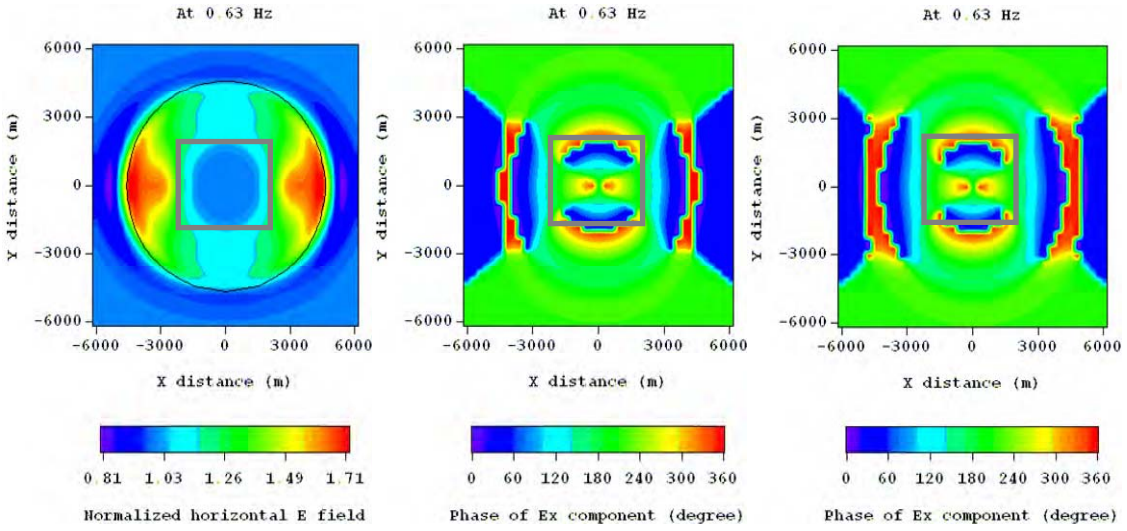

(a) X-oriented HED at (0 m, 0 m, 950 m)

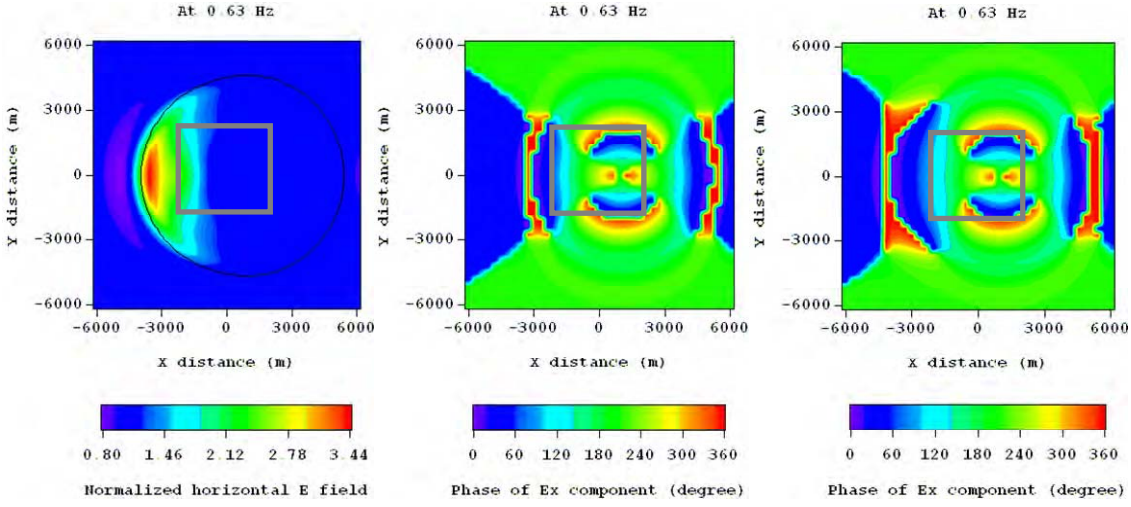

(b) X-oriented HED at (1000 m, 0 m, 950 m)

Figure 5.41. Horizontal electric field responses for the 3-D reservoir model at four different x-oriented HED positions along y=0 m axis. Normalized horizontal electric field plots (left), E_X phase plots for the background model (middle), and E_X phase plots for the 3-D reservoir model (right). The black contours represent the receiver noise level and the grey-colored boxes show the boundary of the 3-D reservoir.

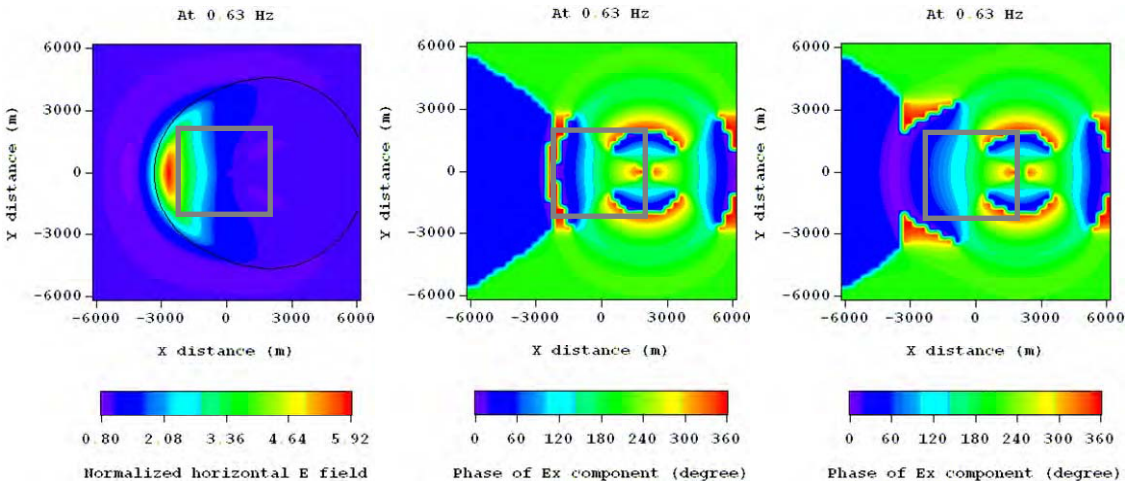

(c) X-oriented HED at (2000 m, 0 m, 950 m)

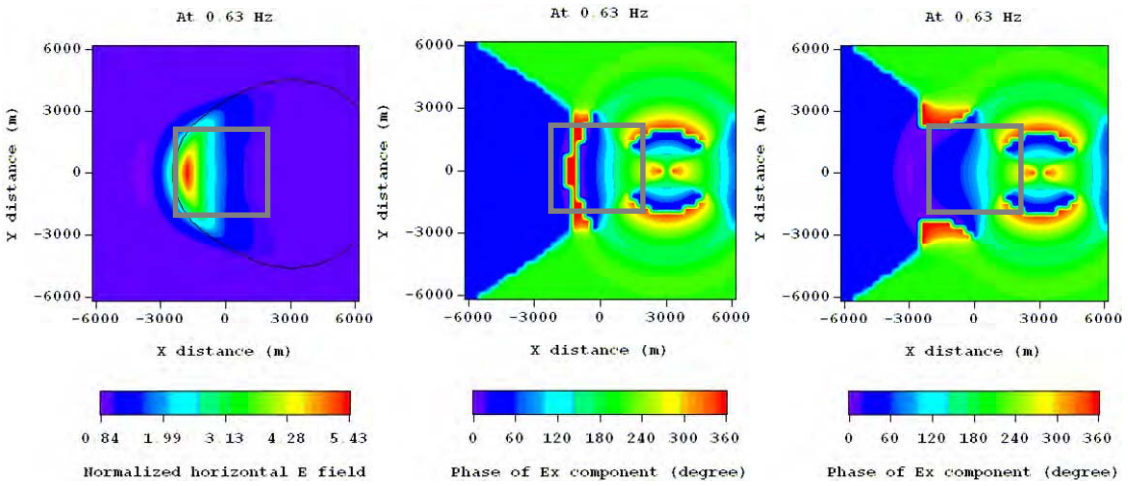

(d) X-oriented HED at (3000 m, 0 m, 950 m)

Figure 5.41. Continued.

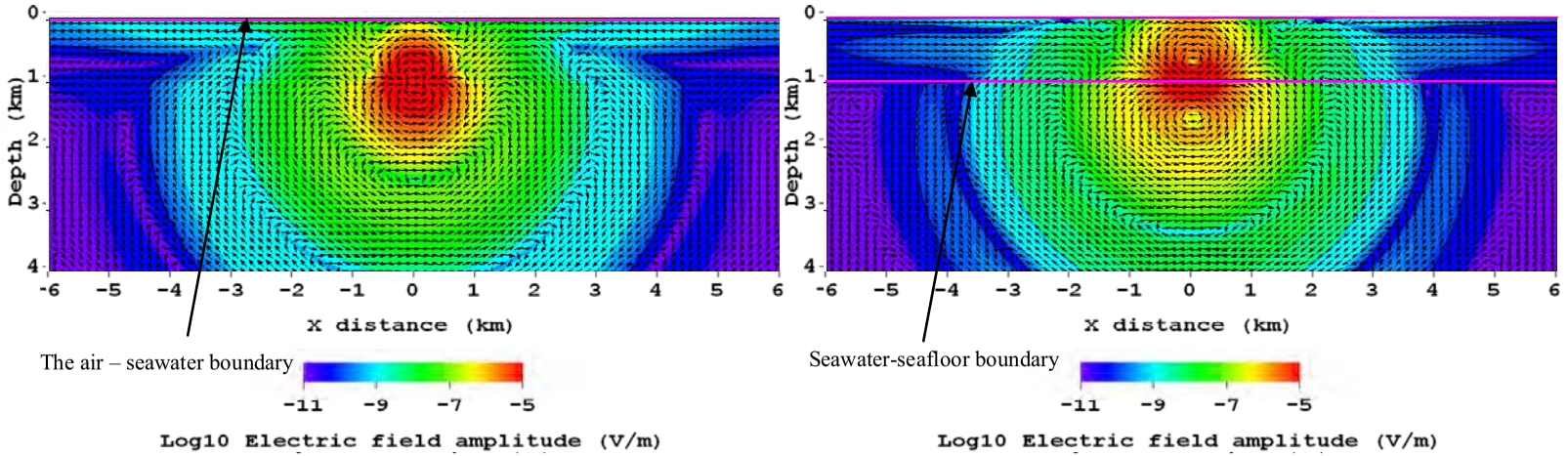

(a) E_{IP} (left) and E_{OP} (right) for the background model with a HED (0 m, 0 m, 950 m)

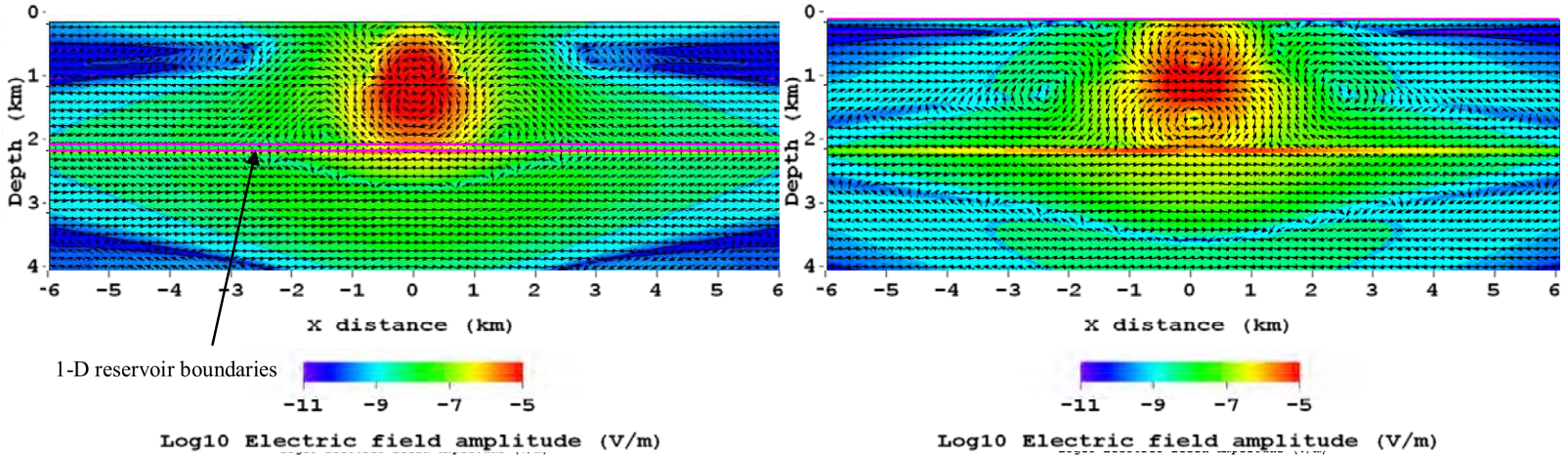

(b) E_{IP} (left) and E_{OP} (right) for the 1-D reservoir model with a HED (0 m, 0 m, 950 m)

Figure 5.42. In-phase and out-of-phase electric field distribution plots with a 0.63 Hz x-oriented HED source for three different models.

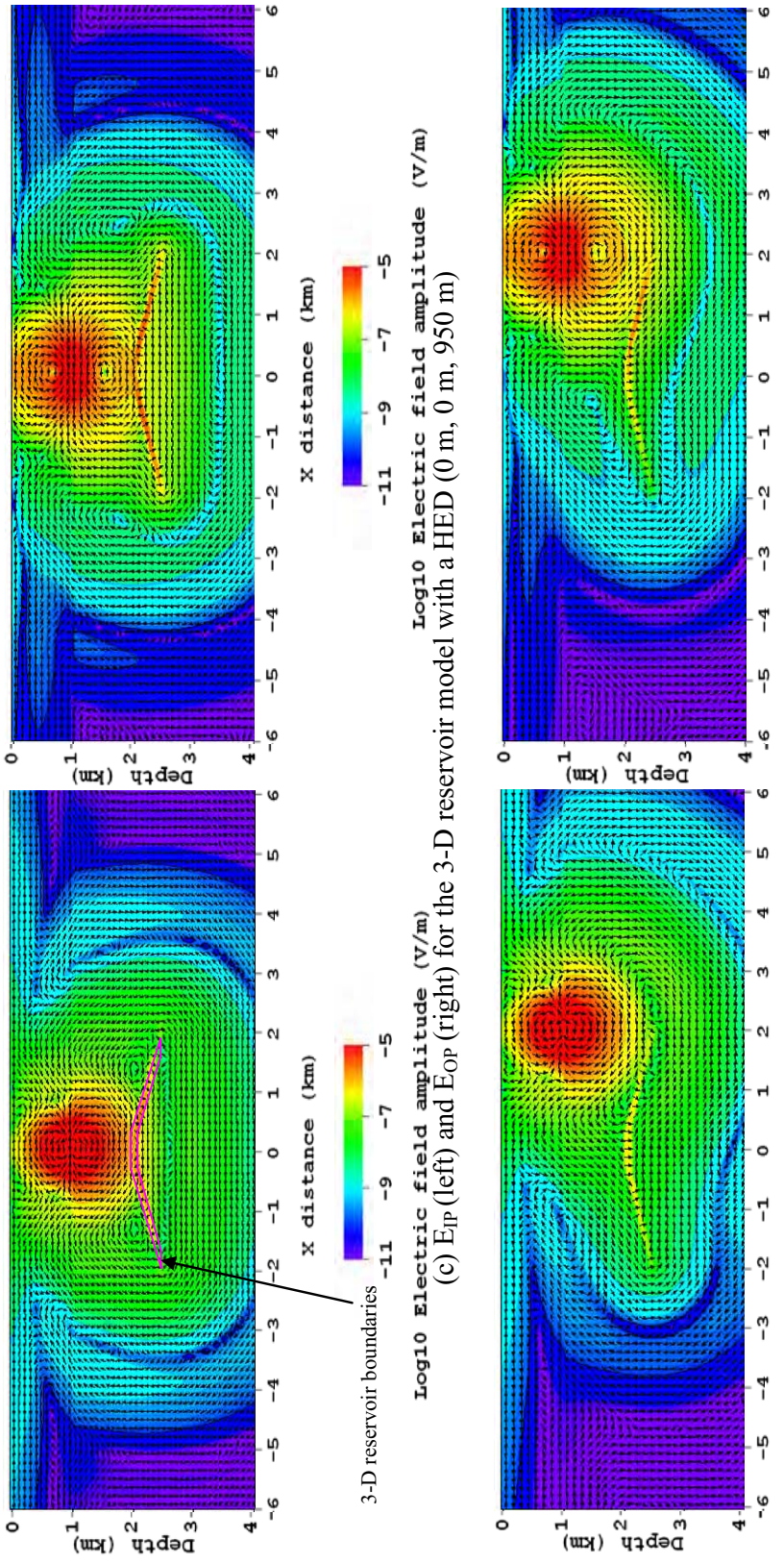

(c) E_{IP} (left) and E_{OP} (right) for the 3-D reservoir model with a HED (0 m, 0 m, 950 m)

(d) E_{IP} (left) and E_{OP} (right) for the 3-D reservoir model with a HED (2000 m, 0 m, 950 m)

Figure 5.42. Continued.

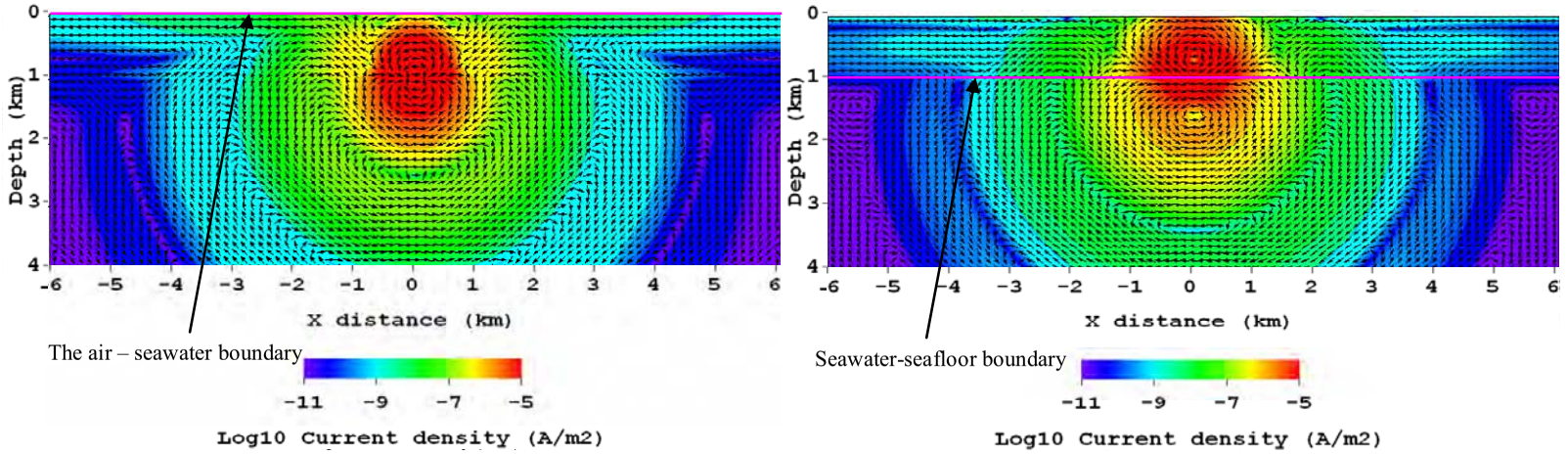

(a) J_{IP} (left) and J_{OP} (right) for the background model with a HED (0 m, 0 m, 950 m)

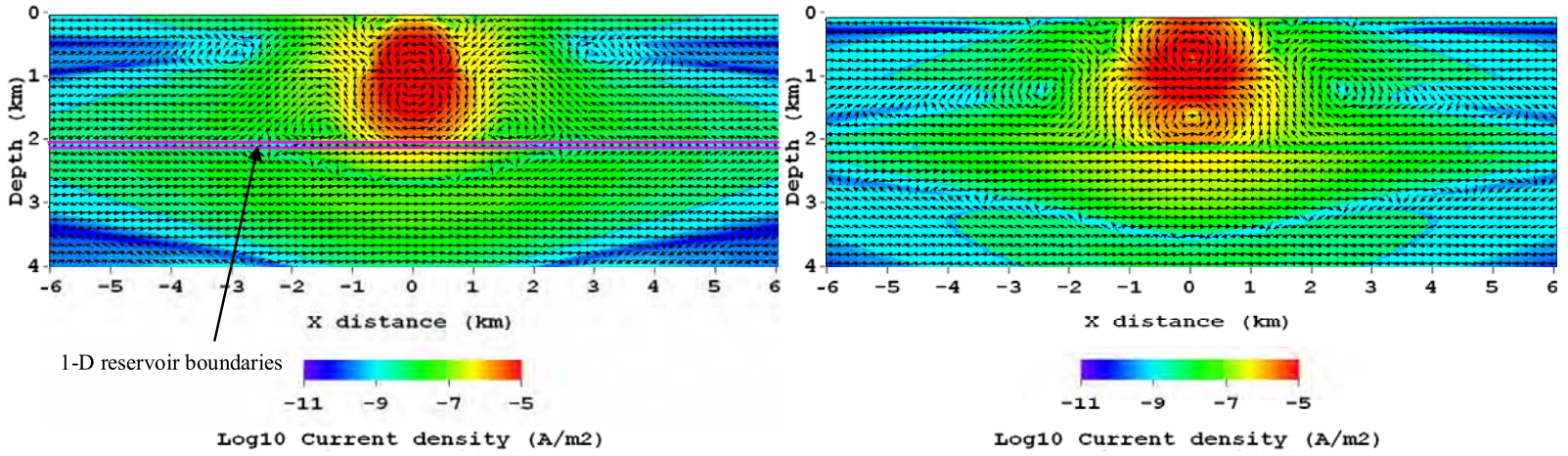

(b) J_{IP} (left) and J_{OP} (right) for the 1-D reservoir model with a HED (0 m, 0 m, 950 m)

Figure 5.43. In-phase and out-of-phase current density distribution plots with a 0.63 Hz x-oriented HED source for three different models.

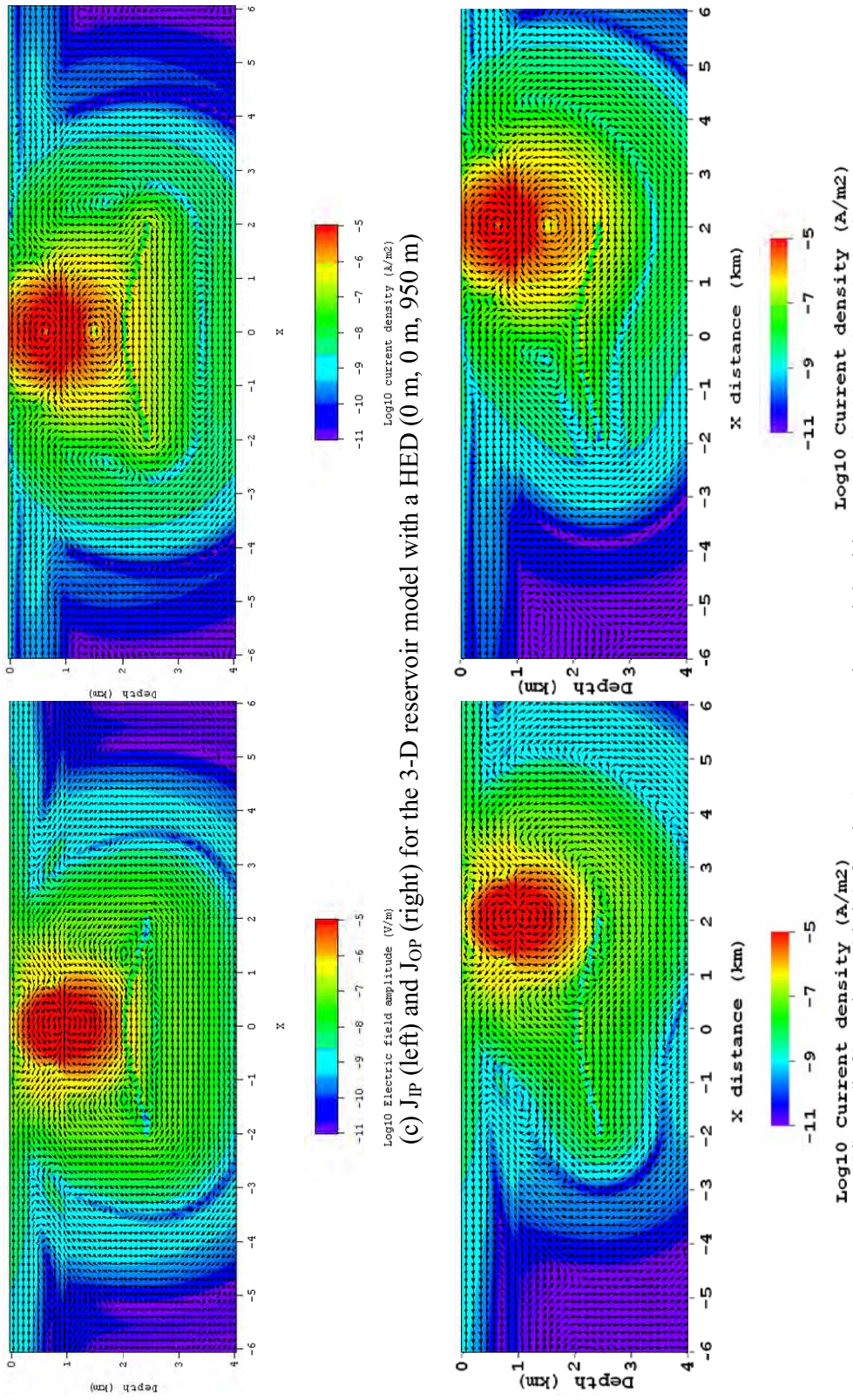

(c) J_{IP} (left) and J_{OP} (right) for the 3-D reservoir model with a HED (0 m, 0 m, 950 m)

(d) J_{IP} (left) and J_{OP} (right) for the 3-D reservoir model with a HED (2000 m, 0 m, 950 m)

Figure 5.43. Continued.

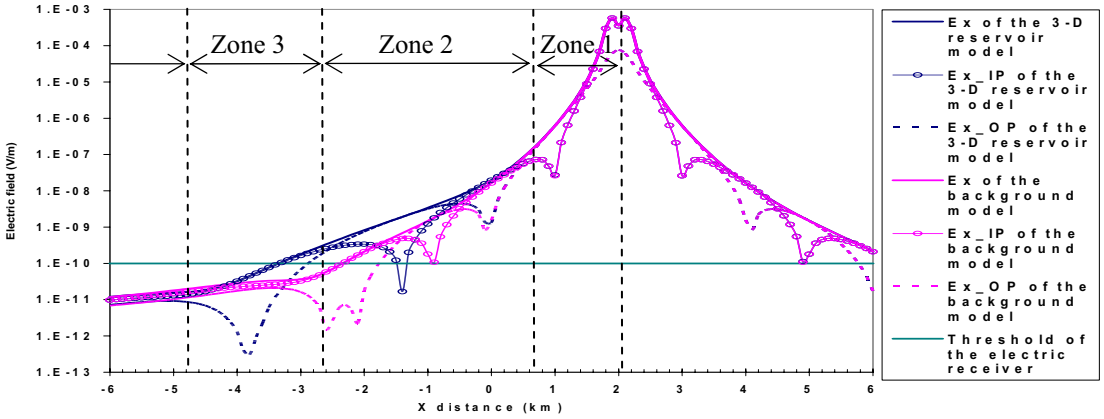

(a) The in-line Ex responses

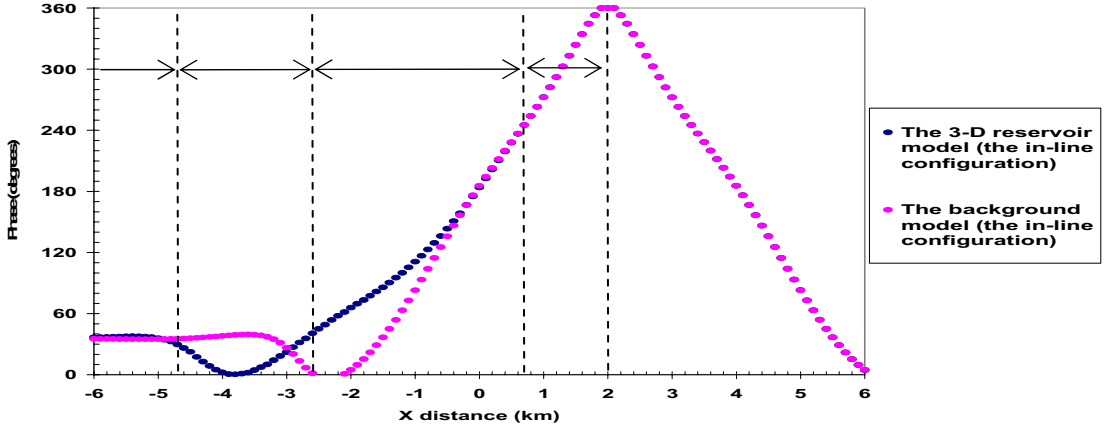

(b) The phase of the Ex components

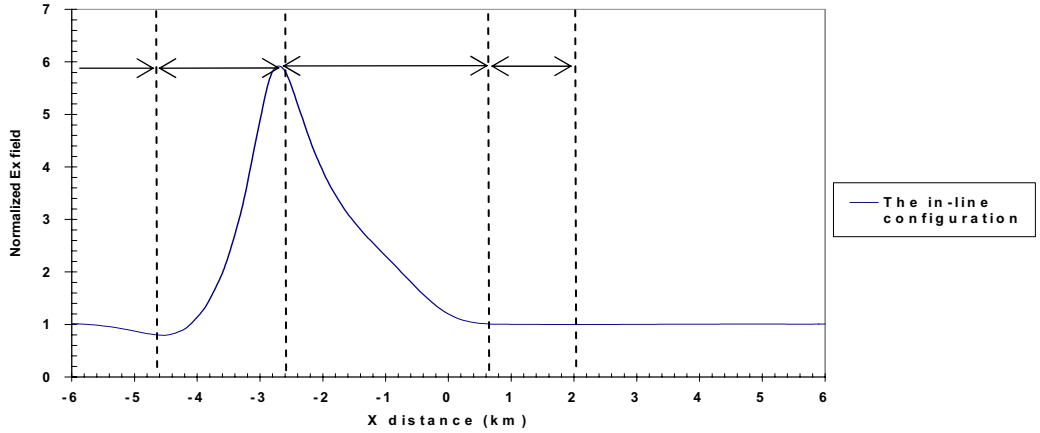

(c) The normalized Ex response

Figure 5.44. Electric field responses for the 3-D reservoir and background models along the y=0 survey line with the x-oriented HED at (2000 m, 0 m, 950 m)

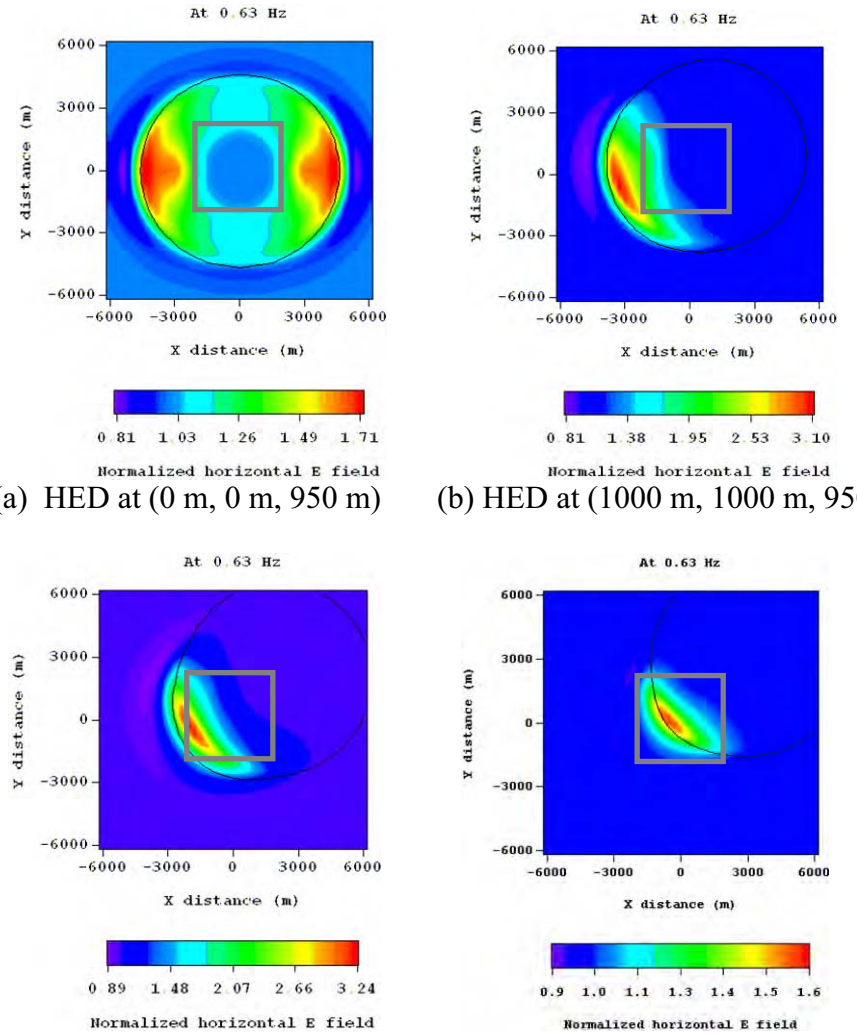

(a) HED at (0 m, 0 m, 950 m) (b) HED at (1000 m, 1000 m, 950 m)

(c) HED at (2000 m, 2000 m, 950 m) (d) HED at (3000 m, 3000 m, 950 m)

Figure 5.45. Normalized horizontal electric field responses with a x-oriented HED source along the diagonal survey line shown in Figure 5.37b. The grey-colored boxes show the boundary of the 3-D reservoir.

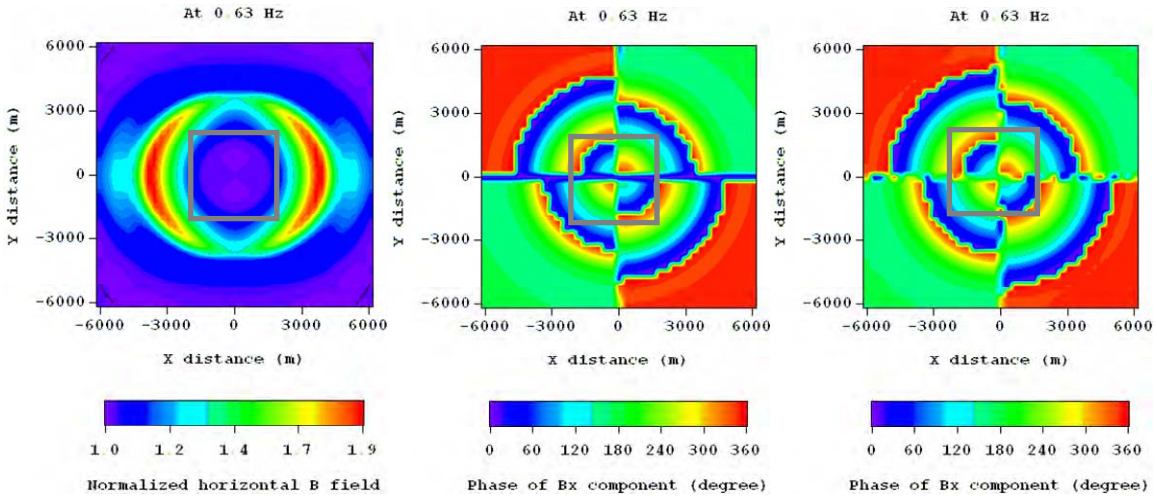

(a) X-oriented HED at (0 m, 0 m, 950 m)

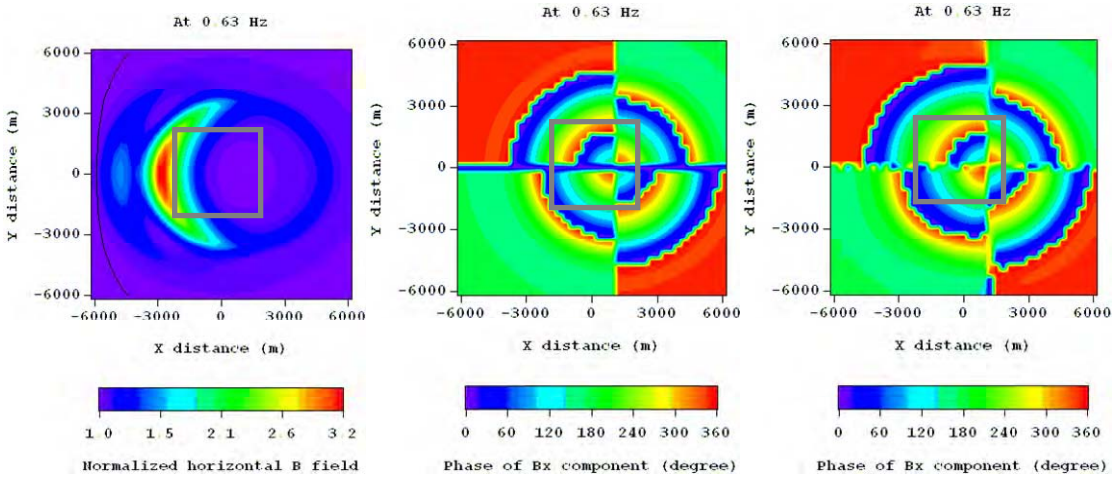

(b) X-oriented HED at (1000 m, 0 m, 950 m)

Figure 5.46. Horizontal magnetic field responses at four different x-oriented HED positions along the x-axis. Normalized horizontal magnetic field plots (left), B_X phase plots of the background model (middle) and B_X phase plots of the 3-D reservoir model (right). The black contours represent the receiver noise level and the grey-colored boxes show the boundary of the 3-D reservoir.

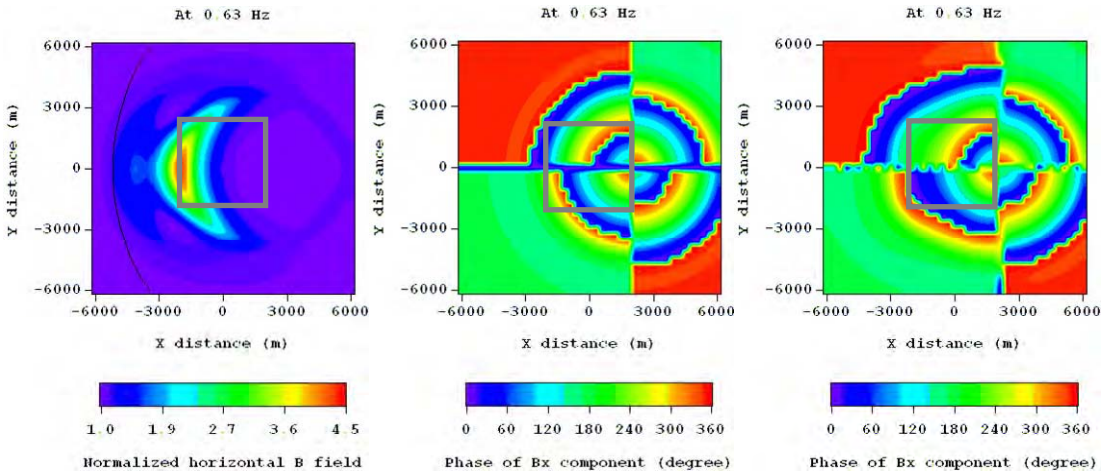

(c) X-oriented HED at (2000 m, 0 m, 950 m)

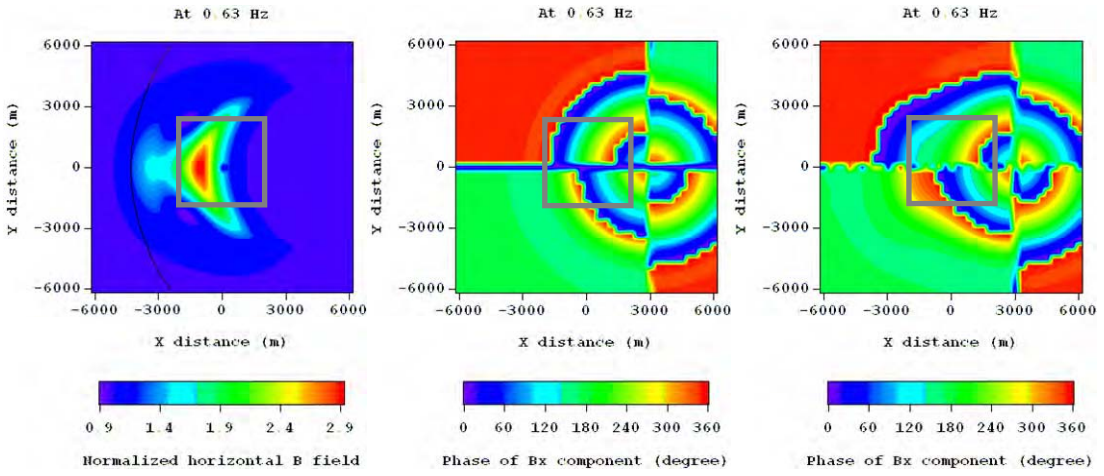

(d) X-oriented HED at (3000 m, 0 m, 950 m)

Figure 5.46. Continued.

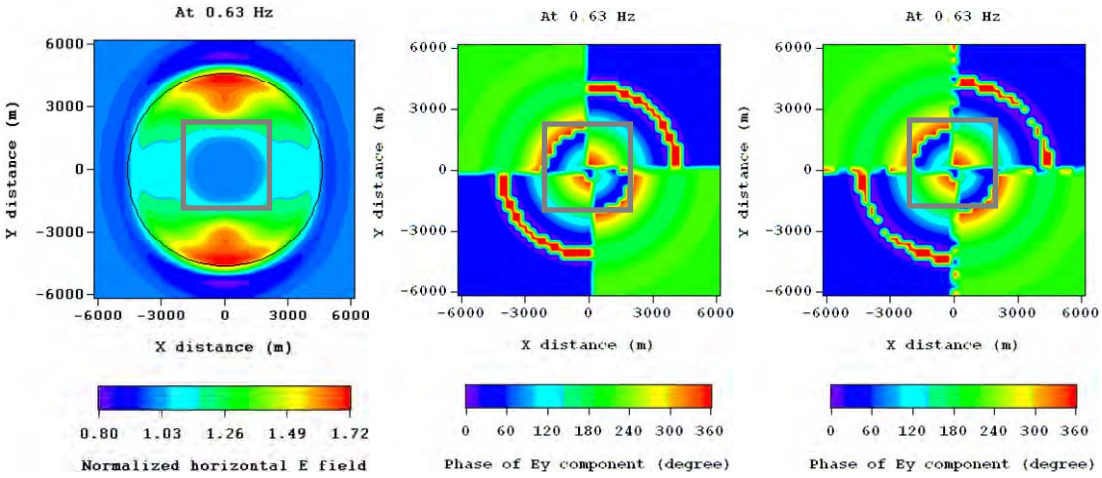

(a) Y-oriented HED at (0 m, 0 m, 950 m)

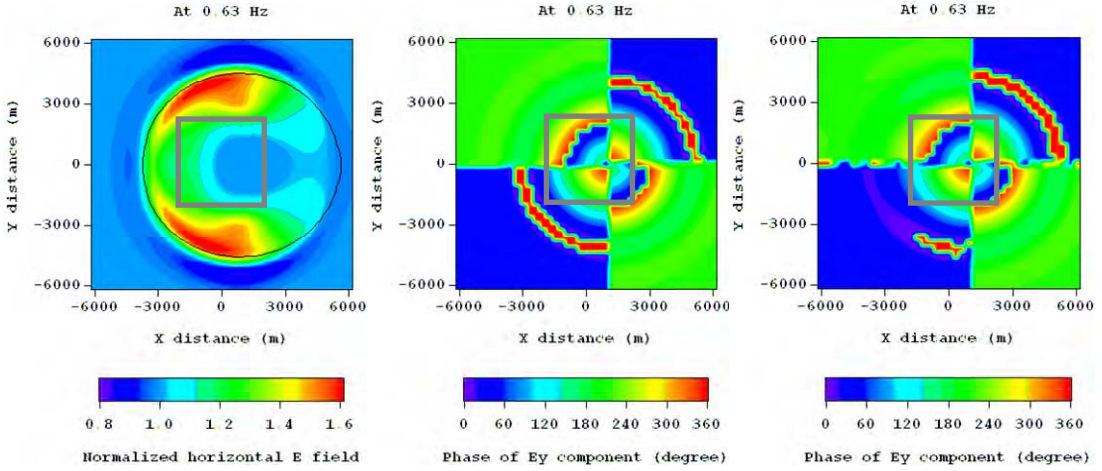

(b) Y-oriented HED at (1000 m, 0 m, 950 m)

Figure 5.47. Horizontal electric field responses at four different y-oriented HED positions along the x axis. Normalized horizontal electric field plots (left), E_Y phase plots of the background model (middle) and E_Y phase plots of the 3-D reservoir model (right). The black contours represent the receiver noise level and the grey-colored boxes show the boundary of the 3-D reservoir.

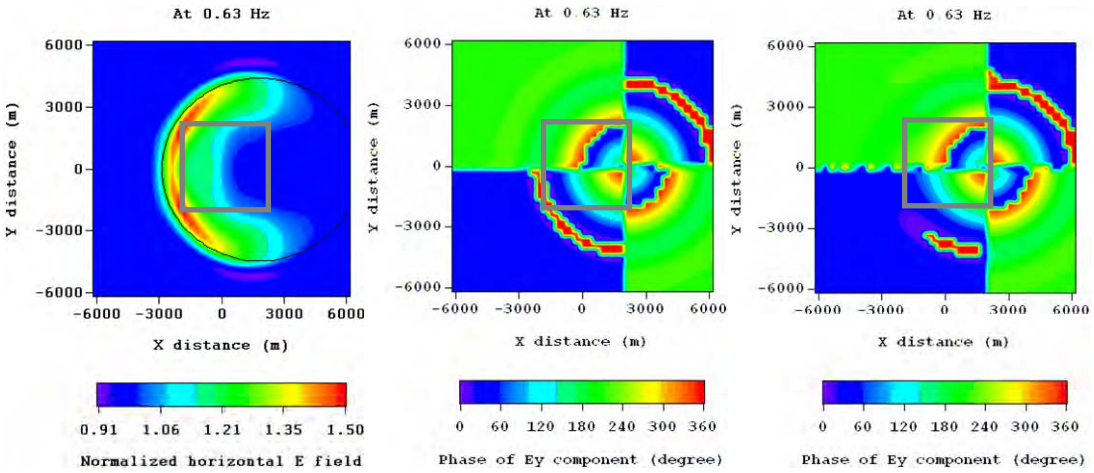

(c) Y-oriented HED at (2000 m, 0 m, 950 m)

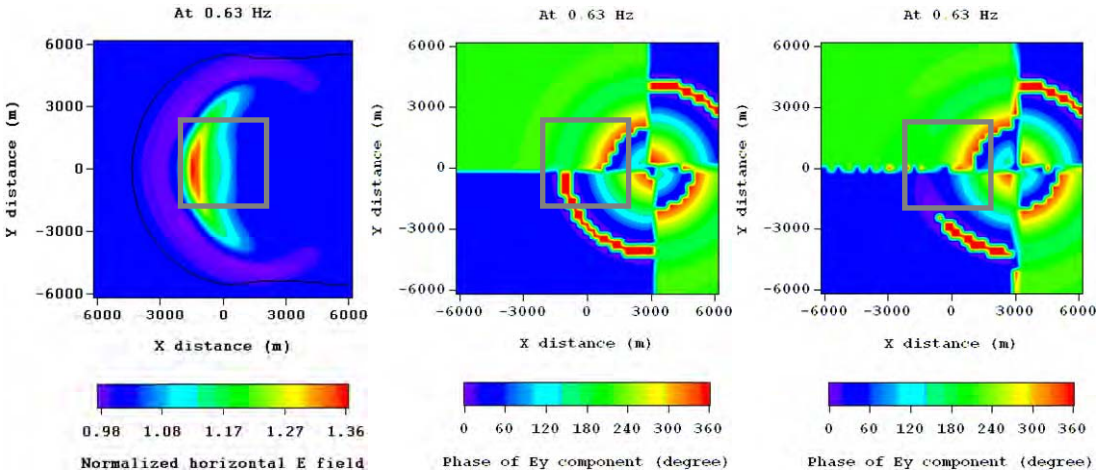

(d) Y-oriented HED at (3000 m, 0 m, 950 m)

Figure 5.47. Continued.

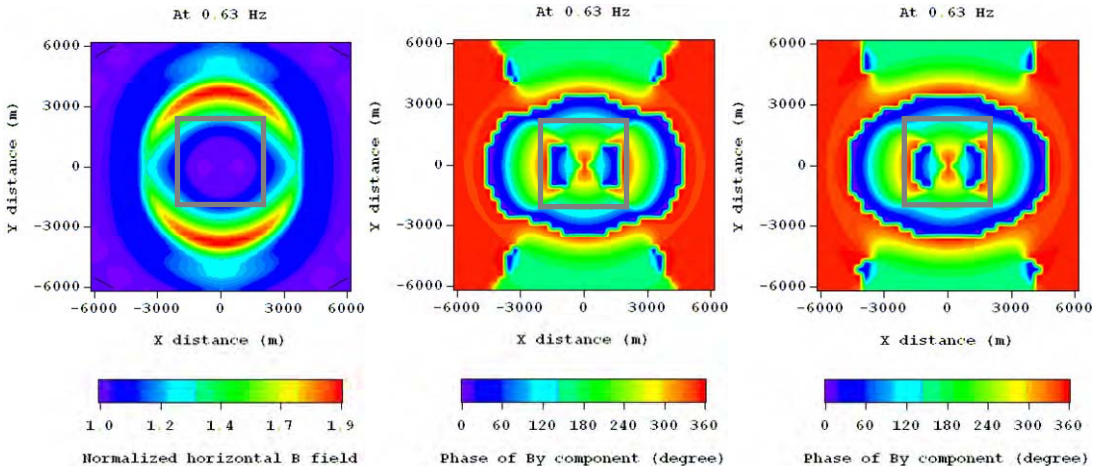

(a) Y-oriented HED at (0 m, 0 m, 950 m)

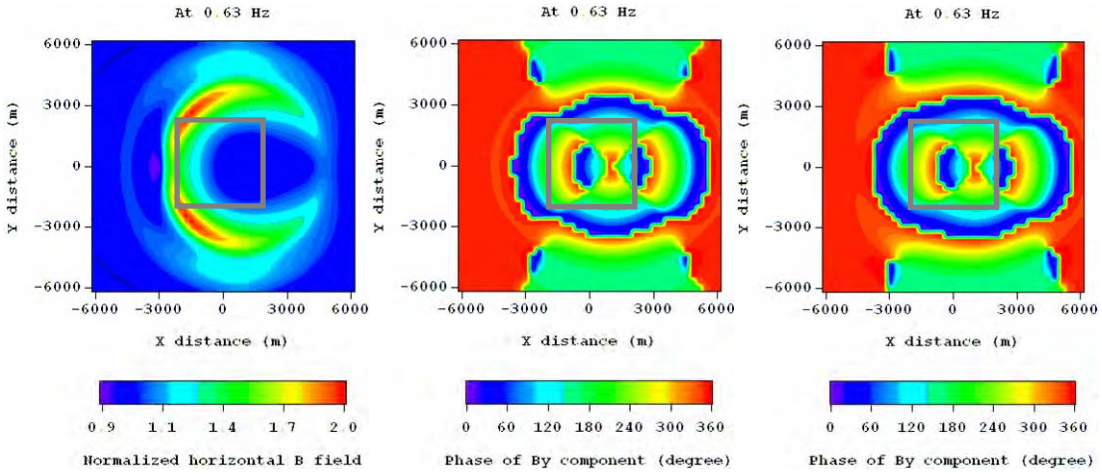

(b) Y-oriented HED at (1000 m, 0 m, 950 m)

Figure 5.48. Horizontal magnetic field responses at four different y-oriented HED positions along the x axis. Normalized horizontal magnetic field plots (left), B_Y phase plots of the background model (middle) and B_Y phase plots of the 3-D reservoir model (right). The black contours represent the receiver noise level and the grey-colored boxes show the boundary of the 3-D reservoir.

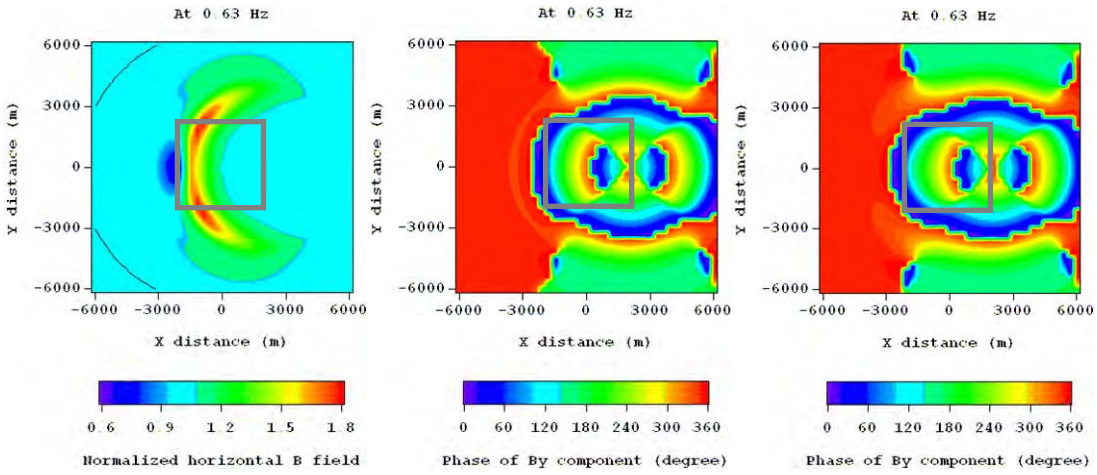

(c) Y-oriented HED at (2000 m, 0 m, 950 m)

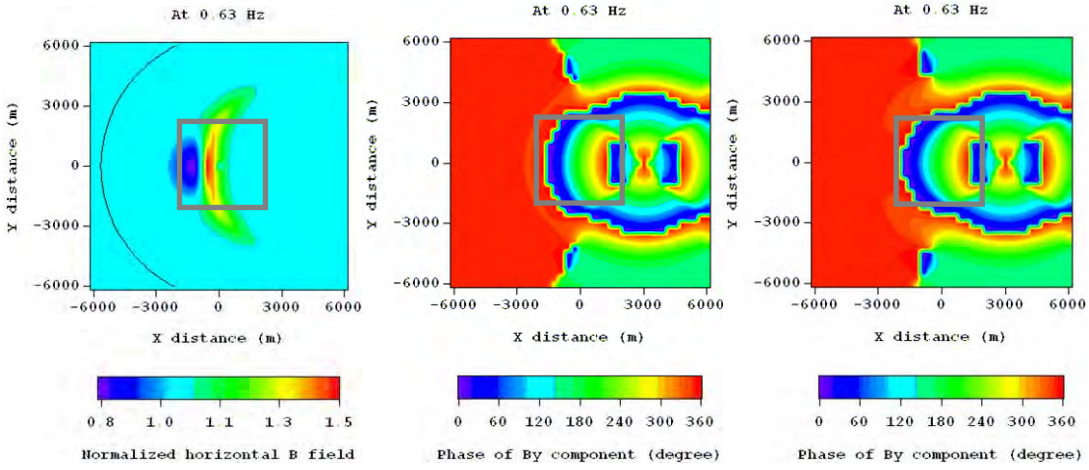

(d) Y-oriented HED at (3000 m, 0 m, 950 m)

Figure 5.48. Continued.

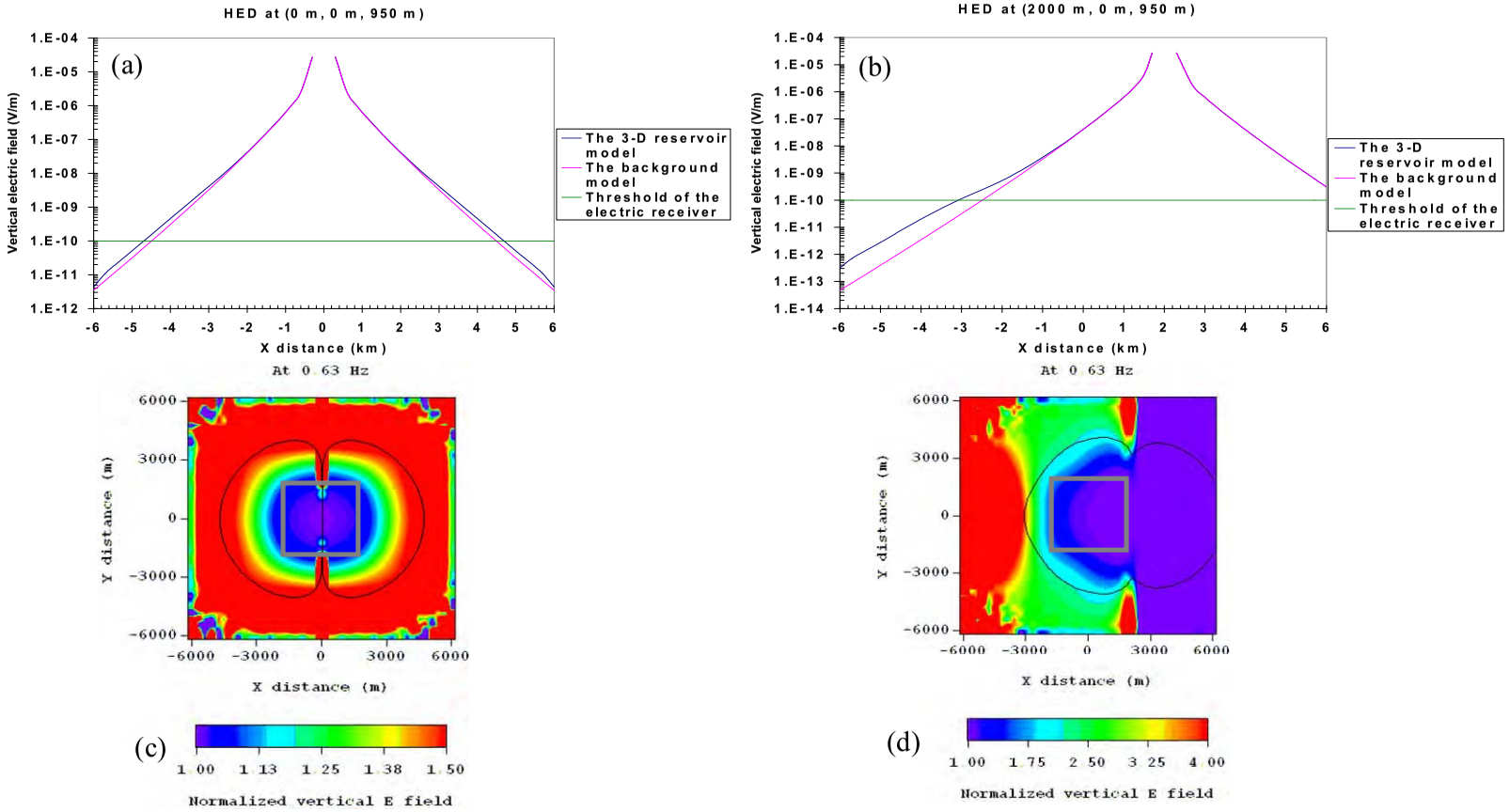

Figure 5.49. E_Z responses over the 3-D reservoir model for the in-line configuration at 0.63 Hz on the seafloor. (a) E_Z responses with an x-oriented HED at (0 m, 0 m and 950 m), (b) E_Z responses with an x-oriented HED at (2000 m, 0 m and 950 m), (c) normalized E_Z response over the 3-D reservoir model with an x-oriented HED at (0 m, 0 m, 950 m), and (d) normalized E_Z response over the 3-D reservoir model with an x-oriented HED at (2000 m, 0 m, 950 m).

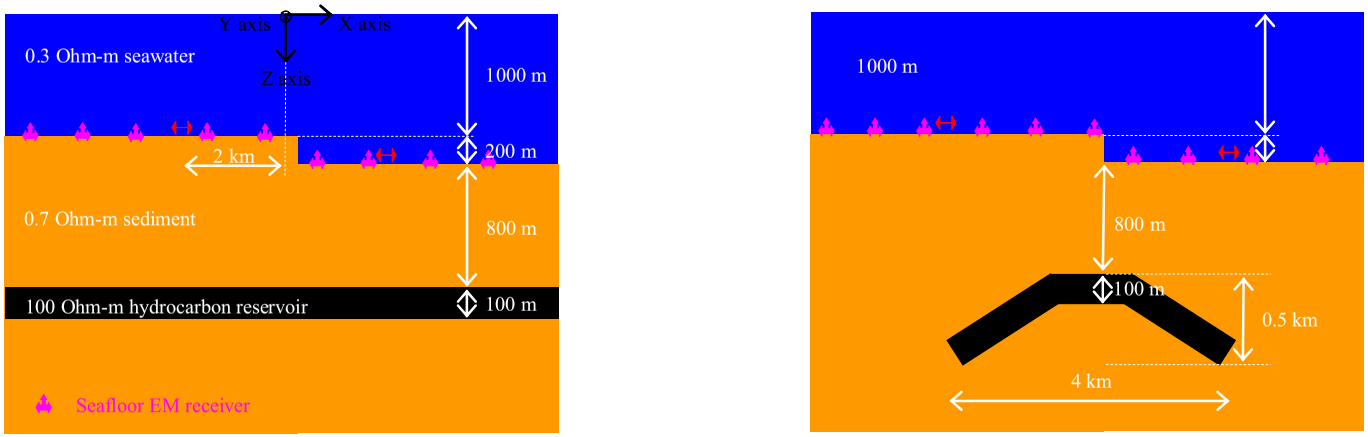

Figure 5.50. The 2-D seafloor topography models. (a) the 1-D reservoir model and (b) the 3-D reservoir model. The red arrows represent HED positions.

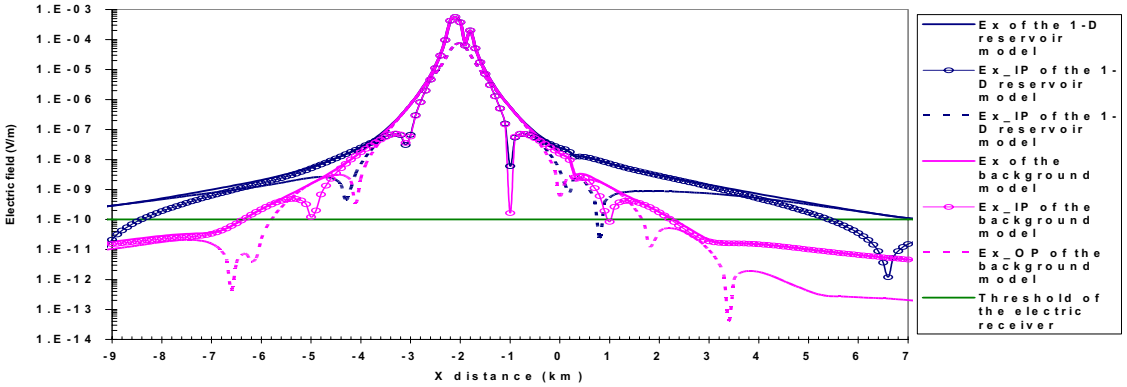

(a) The in-line Ex responses

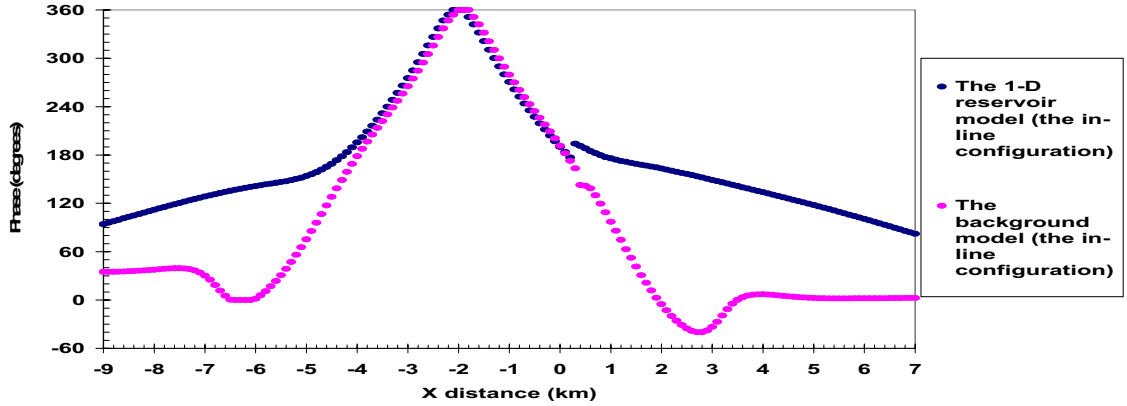

(b) The phases of the Ex components

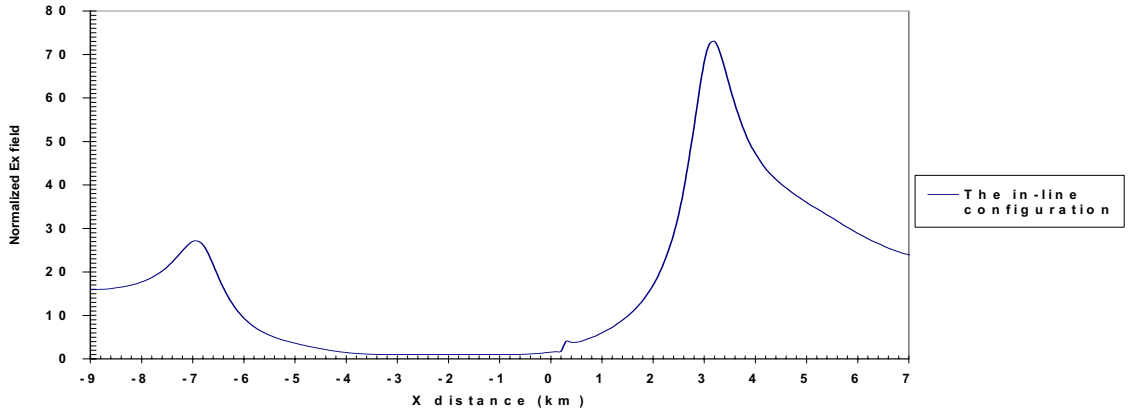

(c) The normalized Ex response

Figure 5.51. E_X responses for the seafloor models having the 2-D seafloor with a 0.63 Hz HED source at (-2000m, 0m, 950m).

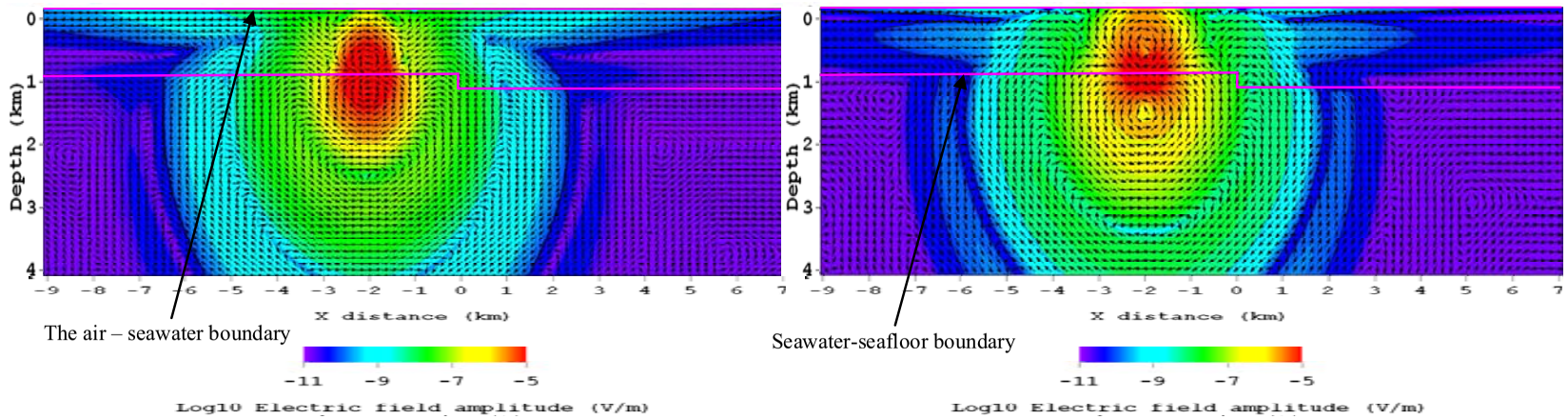

(a) E_{IP} (left) and E_{OP} (right) for the background model

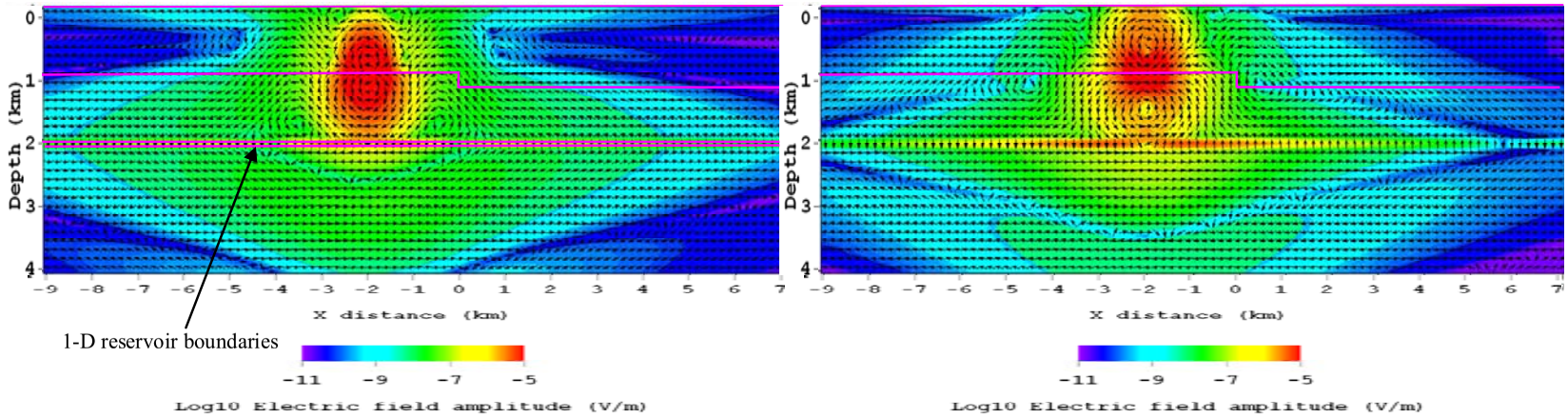

(c) E_{IP} (left) and E_{OP} (right) for the 1-D reservoir model

Figure 5.52. In-phase and out-of-phase E field distribution on the xz plane at y=0(m) for the background model and the 1-D reservoir model with a 0.63 Hz HED source placed at (-2000 m, 0 m, 950 m).

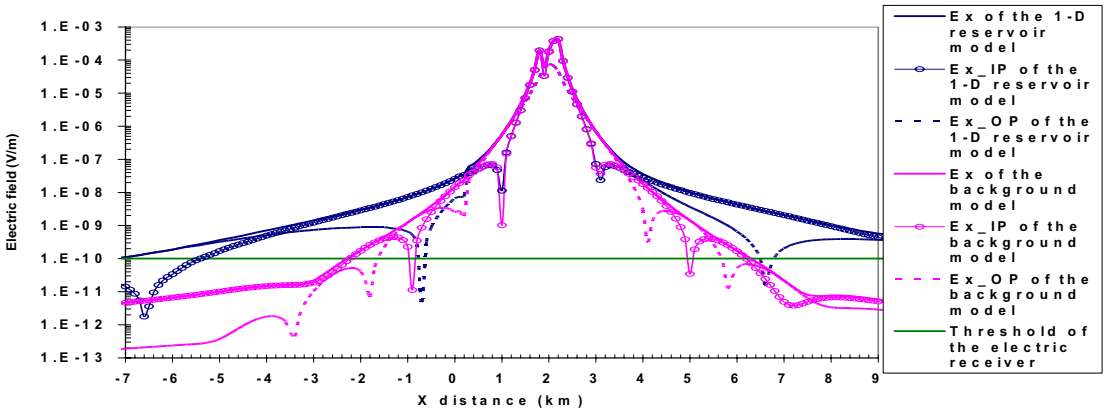

(a) The in-line Ex responses

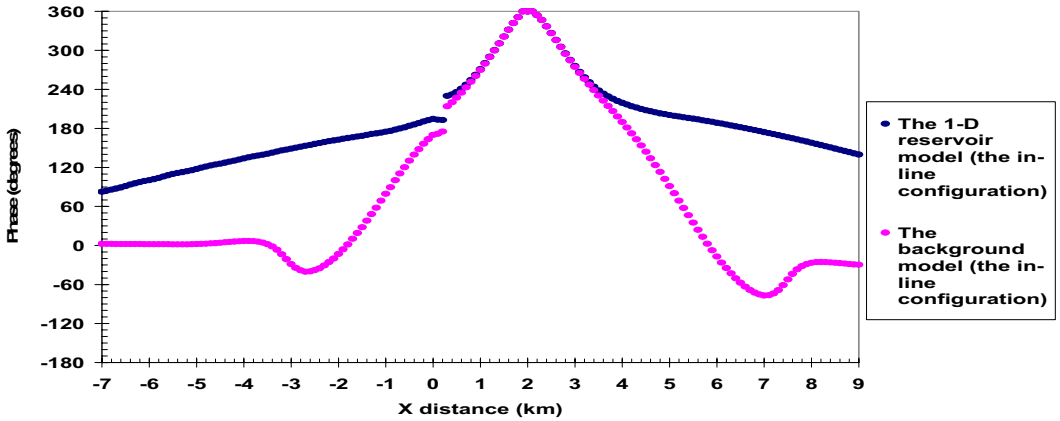

(b) The phases of the Ex components

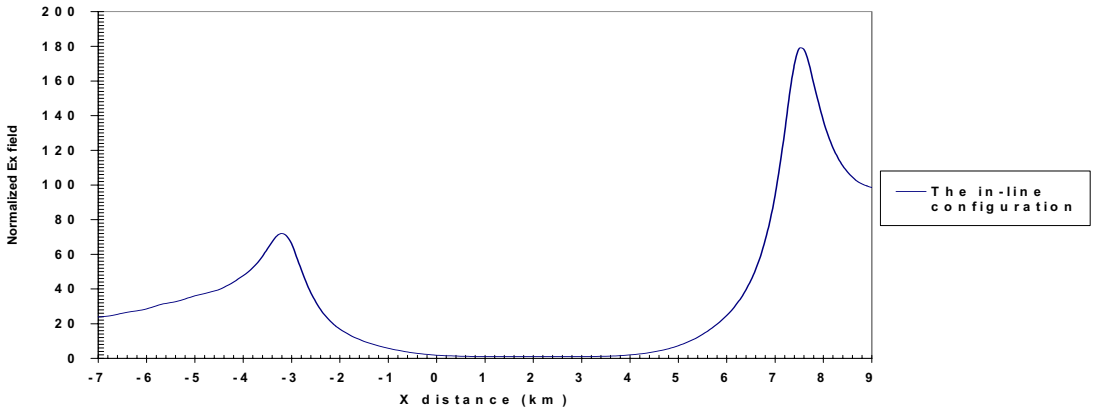

(c) The normalized Ex response

Figure 5.53. E_X responses of the seafloor model having the 2-D seafloor with 0.63 Hz HED at (2000 m, 0 m, 1150 m).

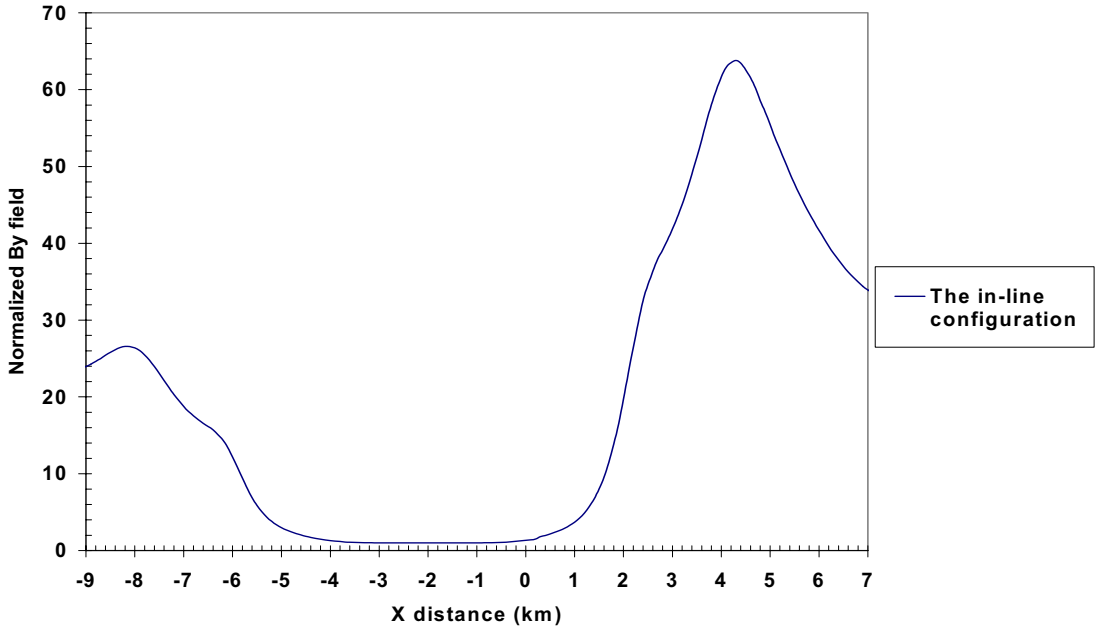

(a) The x-oriented HED at (-2000 m, 0 m, 950 m)

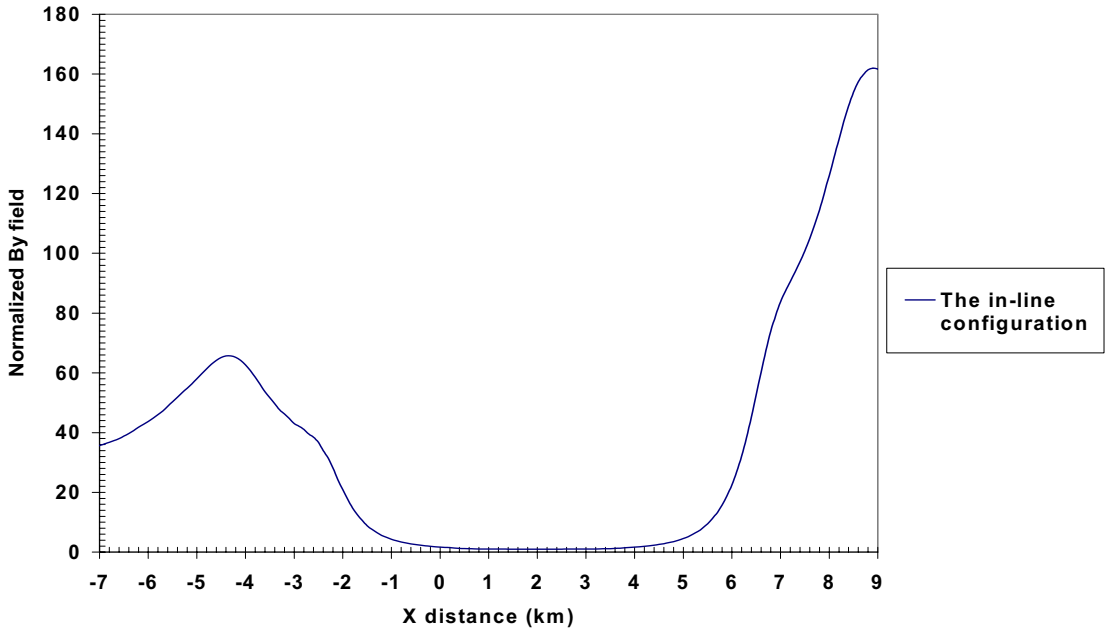

(b) The x-oriented HED at (2000 m, 0 m, 1150 m)

Figure 5.54. The normalized magnetic field responses at 0.63 Hz for the 1-D reservoir model at the two HED positions.

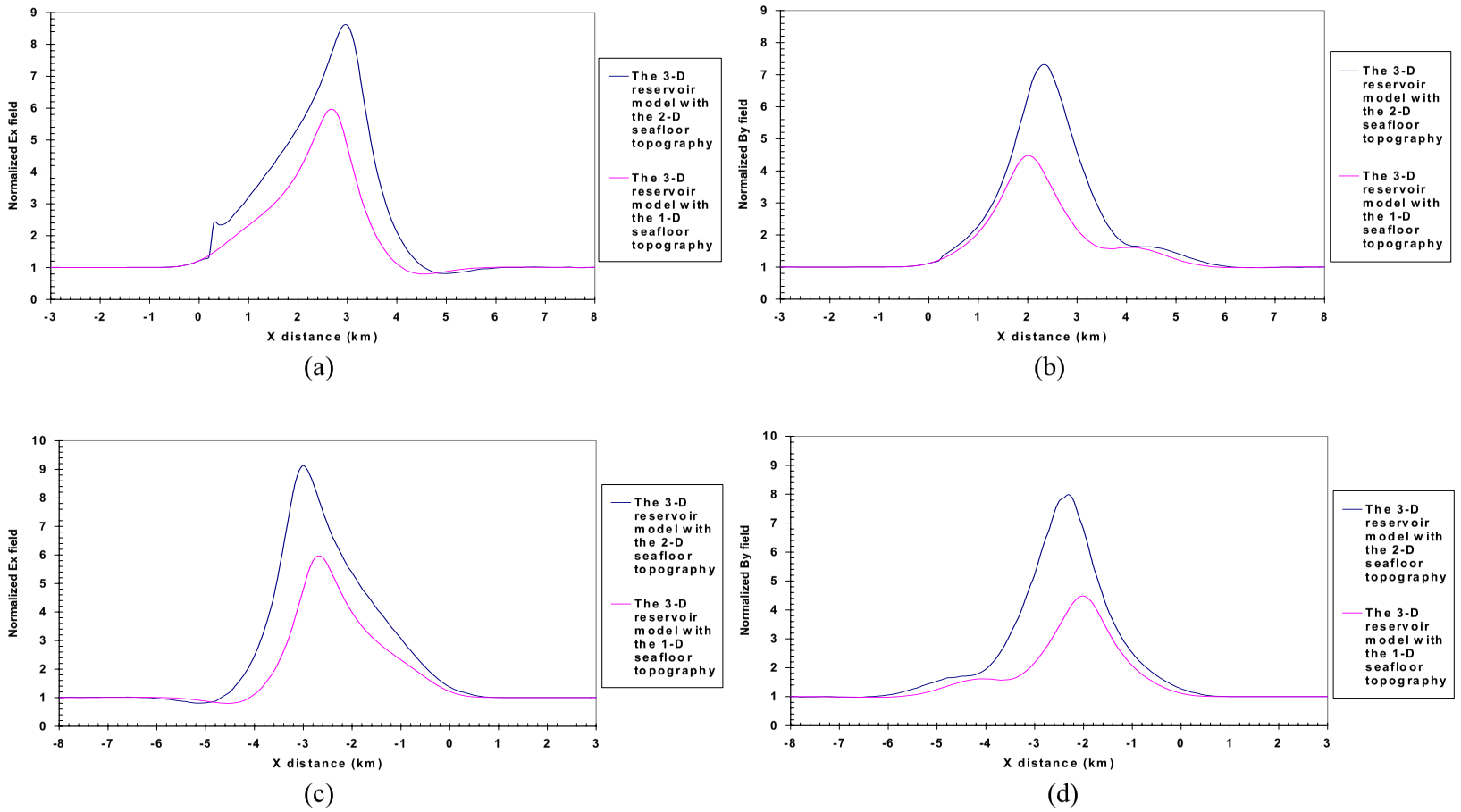

Figure 5.55. Comparison of the 2-D seafloor FDCSEM responses and the 1-D seafloor FDCSEM responses over the 3-D reservoir at 0.63 Hz. The x-oriented HED is 50m above the seafloor. (a) the HED in the 2-D seafloor model: (-2 km, 0 km, 0.95 km), (b) the HED in the 1-D seafloor model: (-2 km, 0 km, 0.95 km), (c) the HED in the 2-D seafloor model: (2 km, 0 km, 1.15 km), and (d) the HED in the 1-D seafloor model: (2 km, 0 km, 0.95 km)

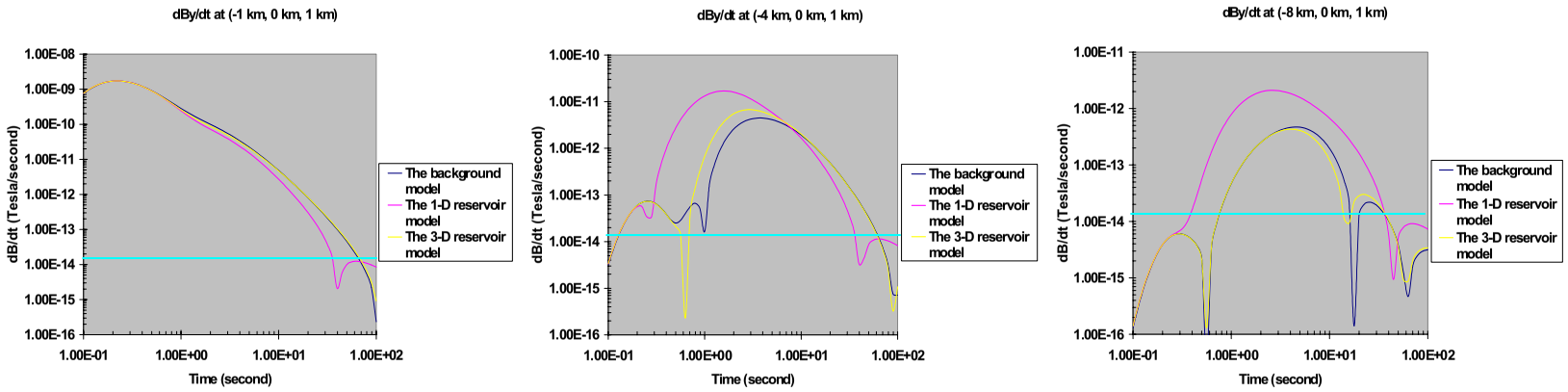

(a) HED position: (0 km, 0 km, 0.95 km)

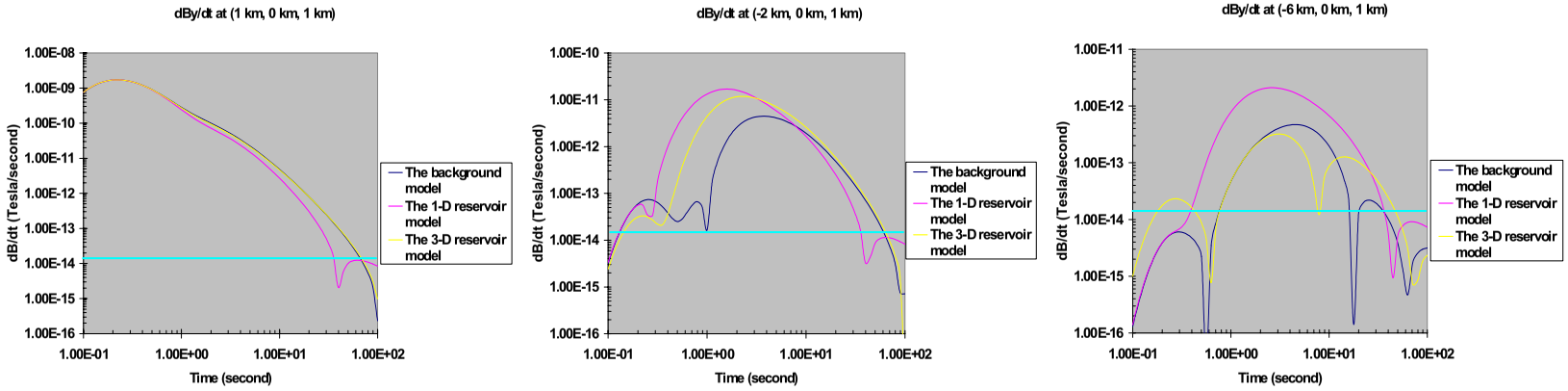

(b) HED position: (2 km, 0 km, 0.95 km)

Figure 5.56. The in-line dB_Y/dt responses using the marine TDCSEM method. Two source positions and three source-receiver Separations are considered. The aqua lines represent the receiver noise level.

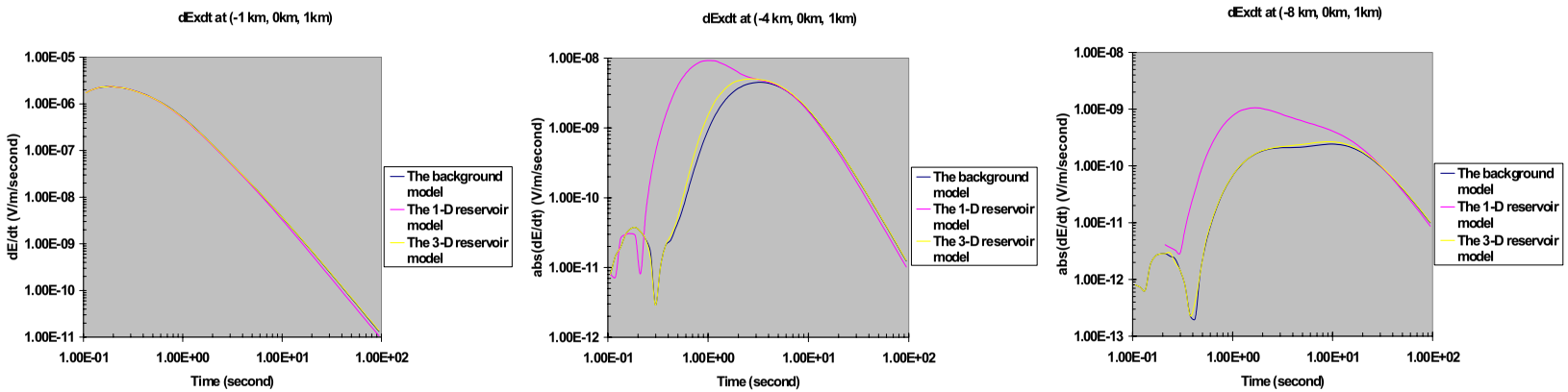

(a) HED position: (0 km, 0 km, 0.95 km)

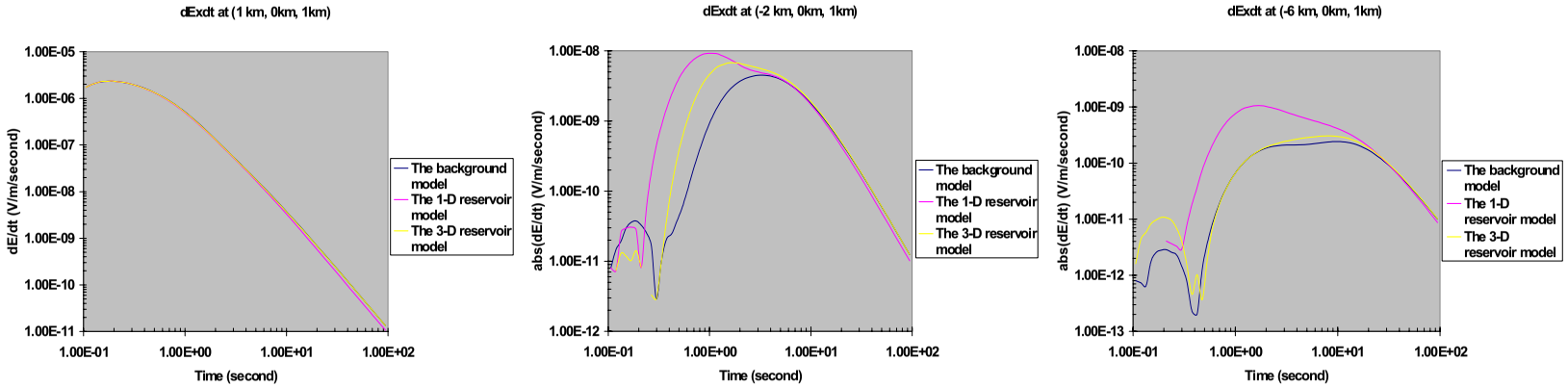

(b) HED position: (2 km, 0 km, 0.95 km)

Figure 5.57. The in-line dE_X/dt responses using the marine TDCSEM method. The two source positions and three source-receiver separations are considered.

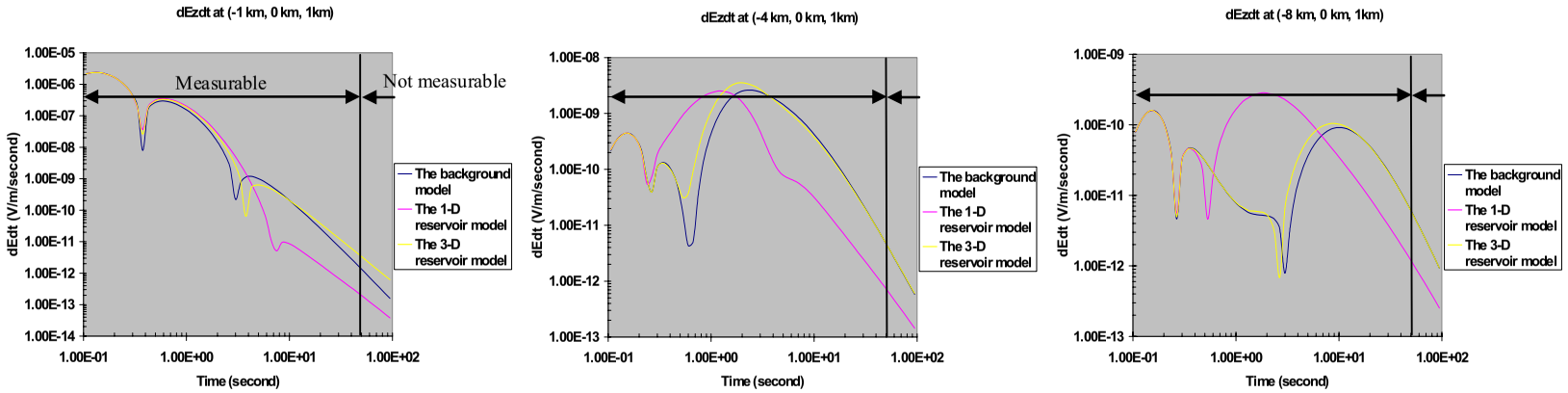

(a) HED position: (0 km, 0 km, 0.95 km)

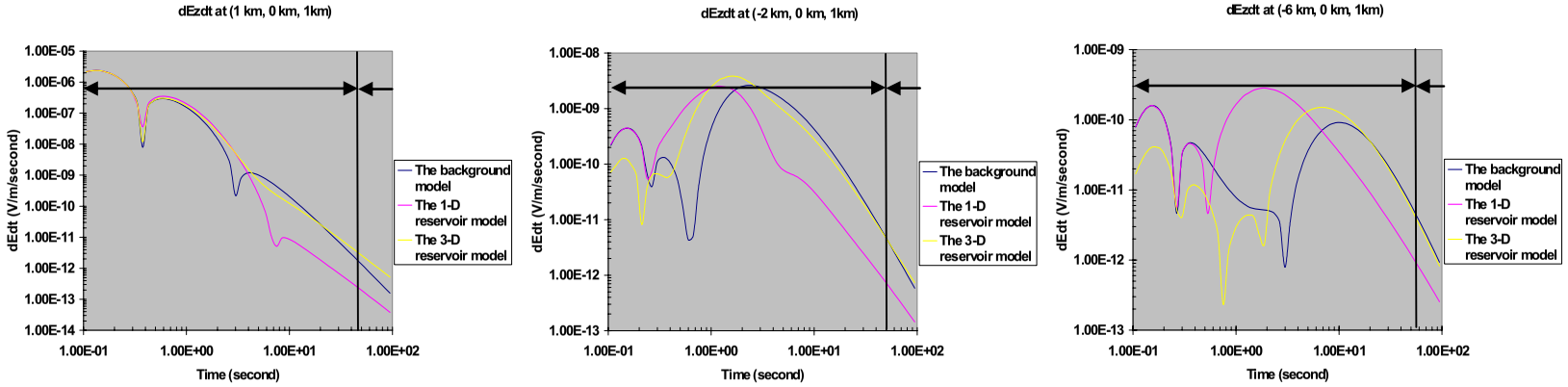

(b) HED position: (2 km, 0 km, 0.95 km)

Figure 5.58. The in-line dE_Z/dt responses using the marine TDCSEM method. The two source positions and three source-receiver separations are considered.

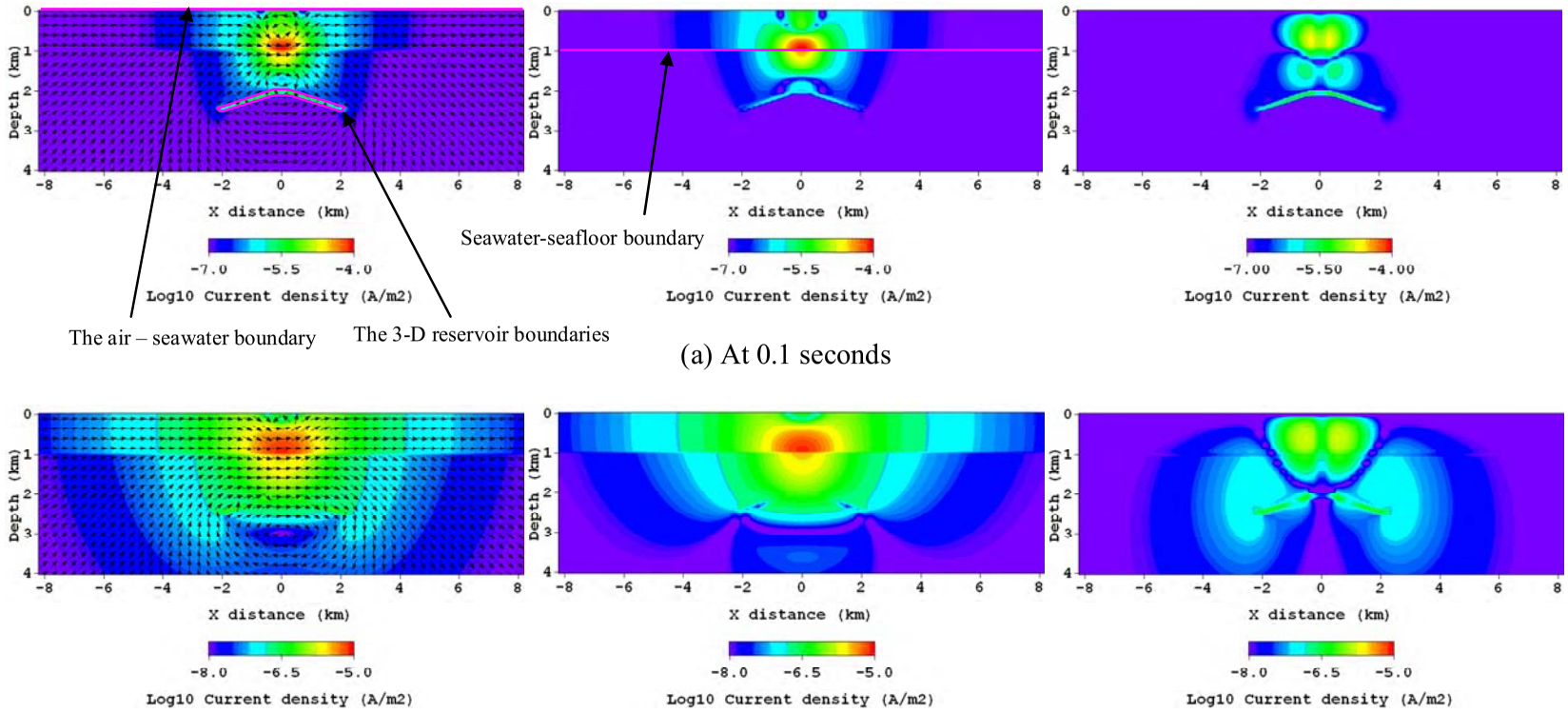

(a) At 0.1 seconds

(b) At 0.5 seconds

Figure 5.59. Current distribution snapshots at four different measurement times on the x-z cross-section for the 3-D reservoir model with a 250m long x-oriented time-domain HED at (0 km, 0 km, 0.95 km). Total current density (left), horizontal current density (middle) and vertical current density (right).

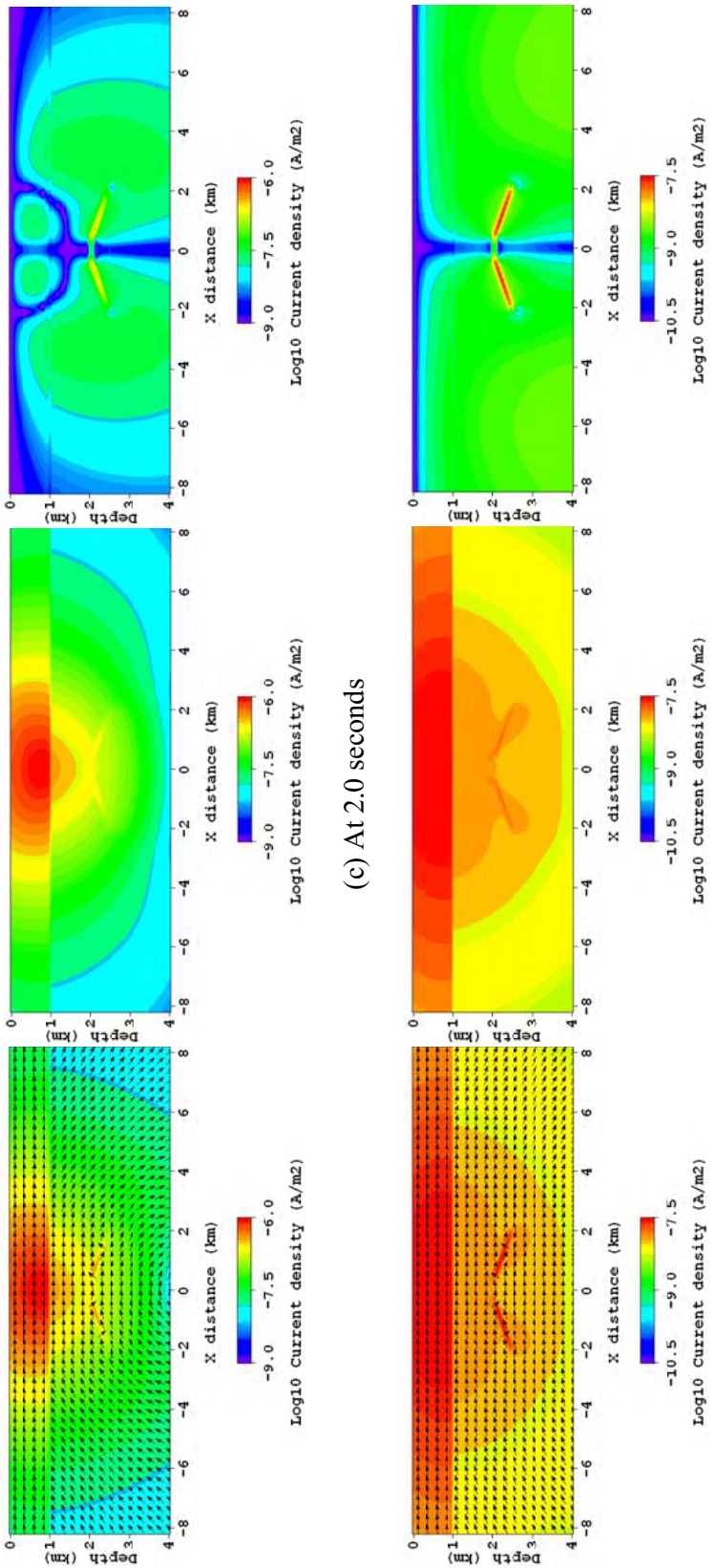

(c) At 2.0 seconds

(d) At 20 seconds

Figure 5.59. Continued.

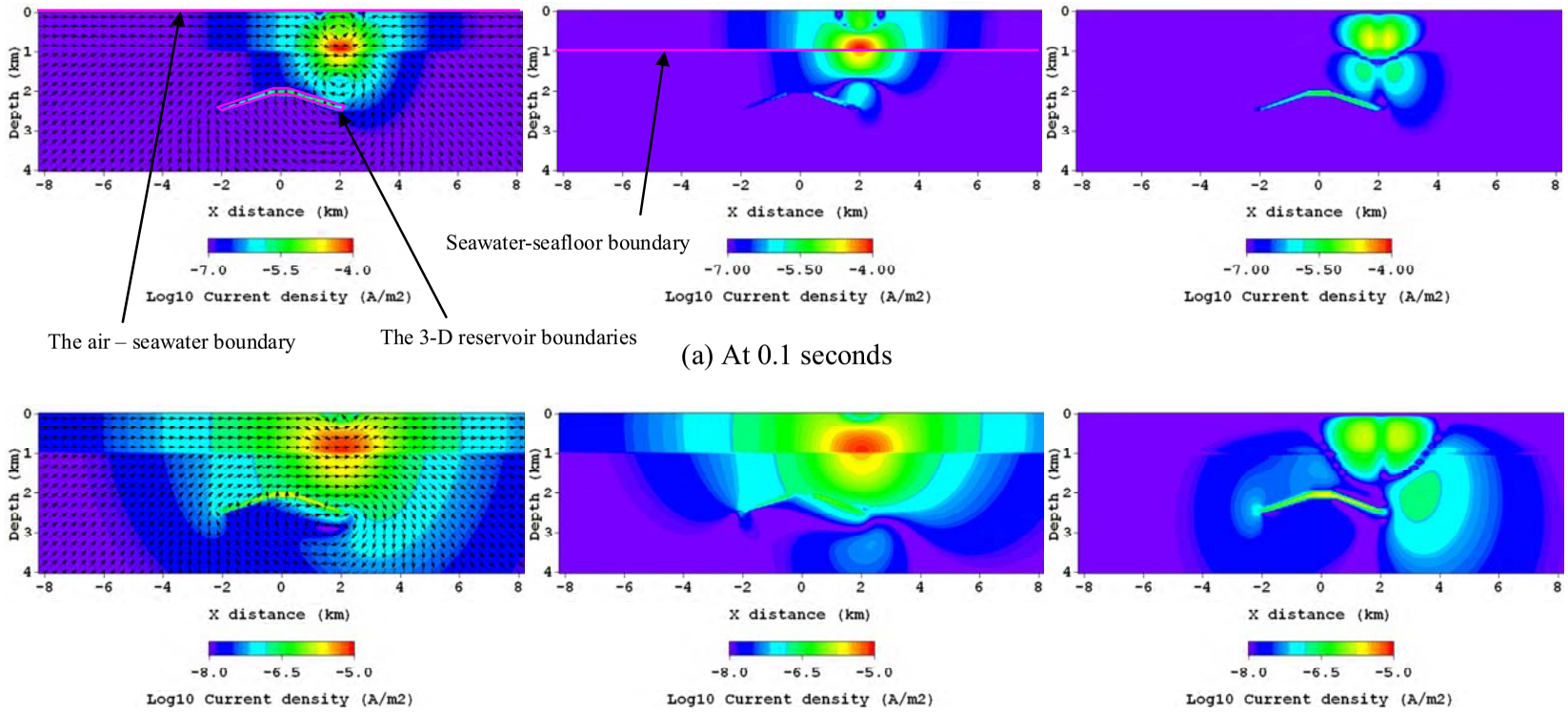

(a) At 0.1 seconds

(b) At 0.5 seconds

Figure 5.60. Current distribution snapshots at four different measurement times on the x-z cross-section for the 3-D reservoir model with a 250m long x-oriented time-domain HED source at (2 km, 0 km, 0.95 km). Total current density (left), horizontal current density (middle) and vertical current density (right).

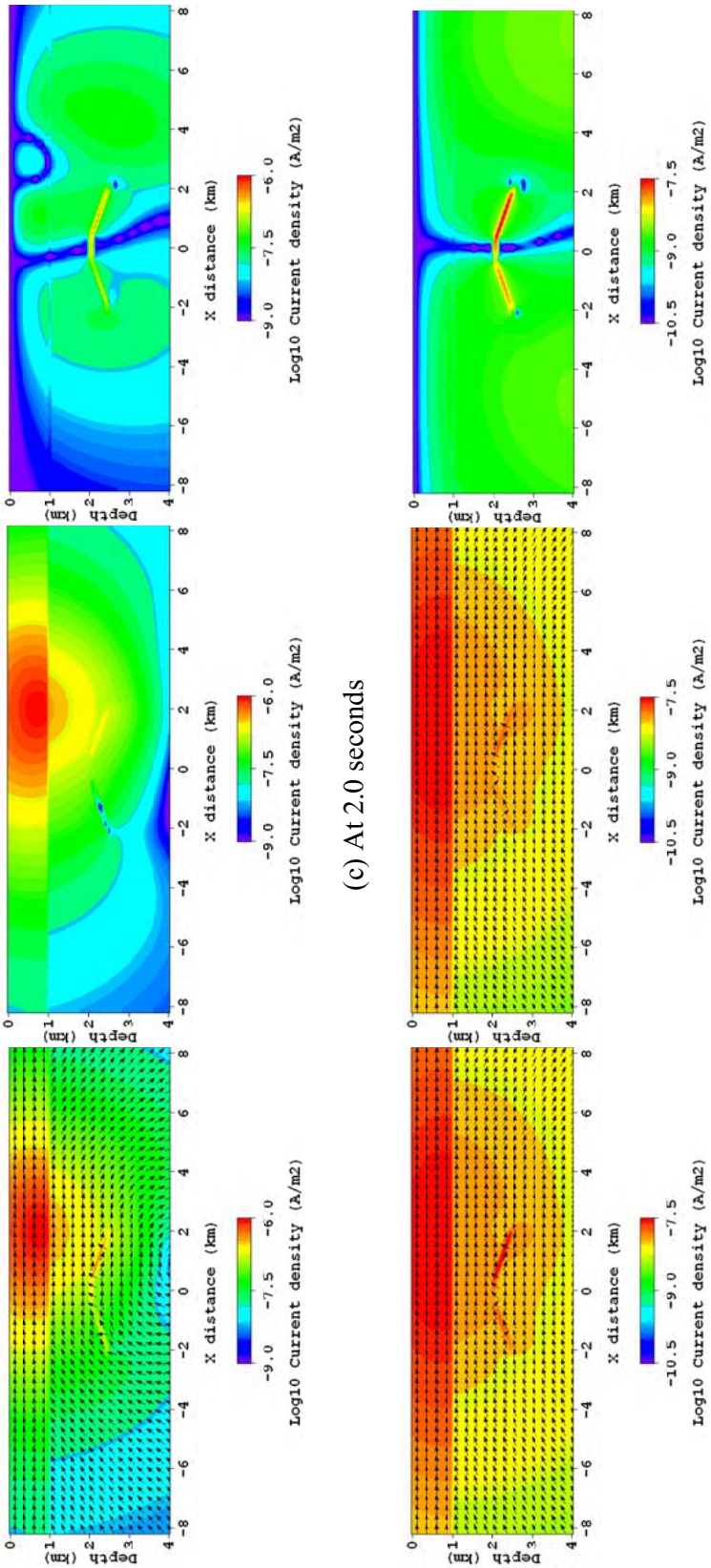

(c) At 2.0 seconds

(d) At 20 seconds

Figure 5.60. Continued.